Department of Physics and Astronomy
Heidelberg University

Bachelor Thesis in Physics
submitted by

Kristian Koehler

born in Elista (Russian Federation)

2022

Inner Bremsstrahlung from leptonic J/ψ decays with ALICE

This Bachelor Thesis has been carried out by Kristian Koehler at the
Physikalisches Institut in Heidelberg
under the supervision of
Priv.-Doz. Dr. Kai Schweda

Abstract

This thesis investigates the feasibility of observing internal bremsstrahlung in the leptonic decay channels of the J/ψ meson to e^+e^- or $\mu^+\mu^-$. The event generator STARlight is used to calculate J/ψ meson production in ultraperipheral Pb-Pb and pp collisions with the recently upgraded ALICE apparatus. by applying Low's theorem the total number of bremsstrahlung photons is calculated. Detector acceptance and efficiencies are taken into account to estimate the number of detected decays of $J/\psi \to l^+l^- + \gamma$. Detailed Monte Carlo studies show that the experimental background in the di-electron channel is an order of magnitude larger than the signal, while the di-muon decay channel is approximately background free. With the full data set of LHC Runs 3 and 4, the total number of detected decays of J/ψ mesons to $\mu^+\mu^-$ together with a bremsstrahlung photon of $E_\gamma > 100\text{MeV}$ is estimated to be about 1000 making such a measurement possible.

Abstract

In dieser Arbeit wird die Möglichkeit der Beobachtung von interner Bremsstrahlung in den leptonischen Zerfallskanälen des J/ψ-Mesons zu e^+e^- oder $\mu^+\mu^-$ untersucht. Der Ereignisgenerator STARlight wird zur Berechnung der Produktion von J/ψ-Mesonen in ultraperipheren Pb-Pb- und pp-Kollisionen mit der kürzlich aufgerüsteten ALICE-Apparatur verwendet. Die Gesamtzahl der Bremsstrahlungsphotonen wird durch Anwendung des Low Theorems berechnet. Detektorakzeptanz und -effizienz werden berücksichtigt, um die Anzahl der nachgewiesenen Zerfälle von $J/\psi \to l^+l^- + \gamma$ zu schätzen. Detaillierte Monte-Carlo-Studien zeigen, dass der experimentelle Hintergrund im Di-Elektronen-Kanal um eine Größenordnung größer ist als das Signal, während der Di-Muonen-Zerfallskanal im Wesentlichen hintergrundfrei ist. Mit dem vollständigen Datensatz der LHC-Läufe 3 und 4 wird die Gesamtzahl der nachgewiesenen Zerfälle von J/ψ-Mesonen zu $\mu^+\mu^-$ zusammen mit einem Bremsstrahlungsphoton von $E_\gamma > 100\text{MeV}$ auf etwa 1000 geschätzt, was eine solche Messung möglich macht.

Contents

Section 1

Introduction

Ever since the introduction of quantum field theory in the last century, many theories regarding soft photons emerged. One of the theories was published in the 1950s by F. Low [1]. In it, he investigates the inner bremsstrahlung radiation in a 2-to-2 scattering process. At sufficiently low photon energies, the emitted photon spectrum can be calculated from the incoming and outgoing charged currents of the non-radiative amplitude. This is a consequence of charge conservation and implemented in quantum field theory as Ward identities.

An experimental violation of Low's theorem would put quantum field theory into a serious crisis. To test this theorem the ALICE collaboration, stationed at the Large Hadron Collider near Geneva, Switzerland, is planning to install a forward conversion tracker (FCT) in the next detector system, which is located in the $3 < \eta < 5$ direction. The FCT has the possibility of measuring the photon transverse momentum down to $k_T \approx 1\text{MeV}$ [2] with installation starting in 2033. Instead of waiting ten years for the first test runs to happen, the possibility might exist to measure and test the theorem for the upcoming Run 3 and Run 4 with the current detector system at ALICE.

The potential process is the leptonic decay of the J/ψ meson, $J/\psi \to l^+l^-$ $(l = e, \mu)$. The J/ψ radiative decay serves as a particular clean test of QED since there is no radiation of photons from the J/ψ meson due to charge conjugation invariance. The vector meson carries a C-parity of -1, as does the photon. This distinguishes the decay channel from, for example, the much more abundant process $\rho \to \pi\pi\gamma$ with hadrons in the final state, where structural radiation is possible. The meson is produced in ultra-peripheral Pb-Pb collisions, which results in the produced J/ψ being nearly at rest. In these collisions, exactly two charged tracks are reconstructed. With the absence of pions, a clean separation of electrons and muons is possible by measuring the specific energy loss dE/dx in the ALICE Time Projection Chamber, as shown in Fig. 1.1. Due to the rather small momentum of the J/ψ of about 100 MeV on average, this decay has a clear experimental signature of two oppositely charged tracks that are pointing back-to-back. With the continuous readout after the ALICE upgrade, every event is now recorded and no hardware trigger must be applied. In LHC Run 1 and 2, from 2009 to 2018, the integrated luminosity of the UPC lead-lead collision type is $L_{int} = 233\mu\text{b}^{-1}$ [3]. For Run 3 and 4 an integrated luminosity for the same interaction type of $L_{int} = 10\text{nb}^{-1}$ is anticipated [5]. Taking into account the increased luminosity and the rather small triggering and reconstruction efficiency for ultra-peripheral collisions in Run 1 and Run 2, a few million reconstructed J/ψ mesons are expected in the dilepton channels for the complete Run 3 and Run 4 data set. Within this thesis, the UPC process is simulated using the event generator "STARlight", which was introduced to simulate such interaction types. The information gained from the simulated data is inserted into Low's formula to compute the photon number density. The lower limit is set by the capability of measuring the photon via conversion to electron-positron pairs in the detector material in front of the TPC. The computed results are also compared to experimental and theoretical data to
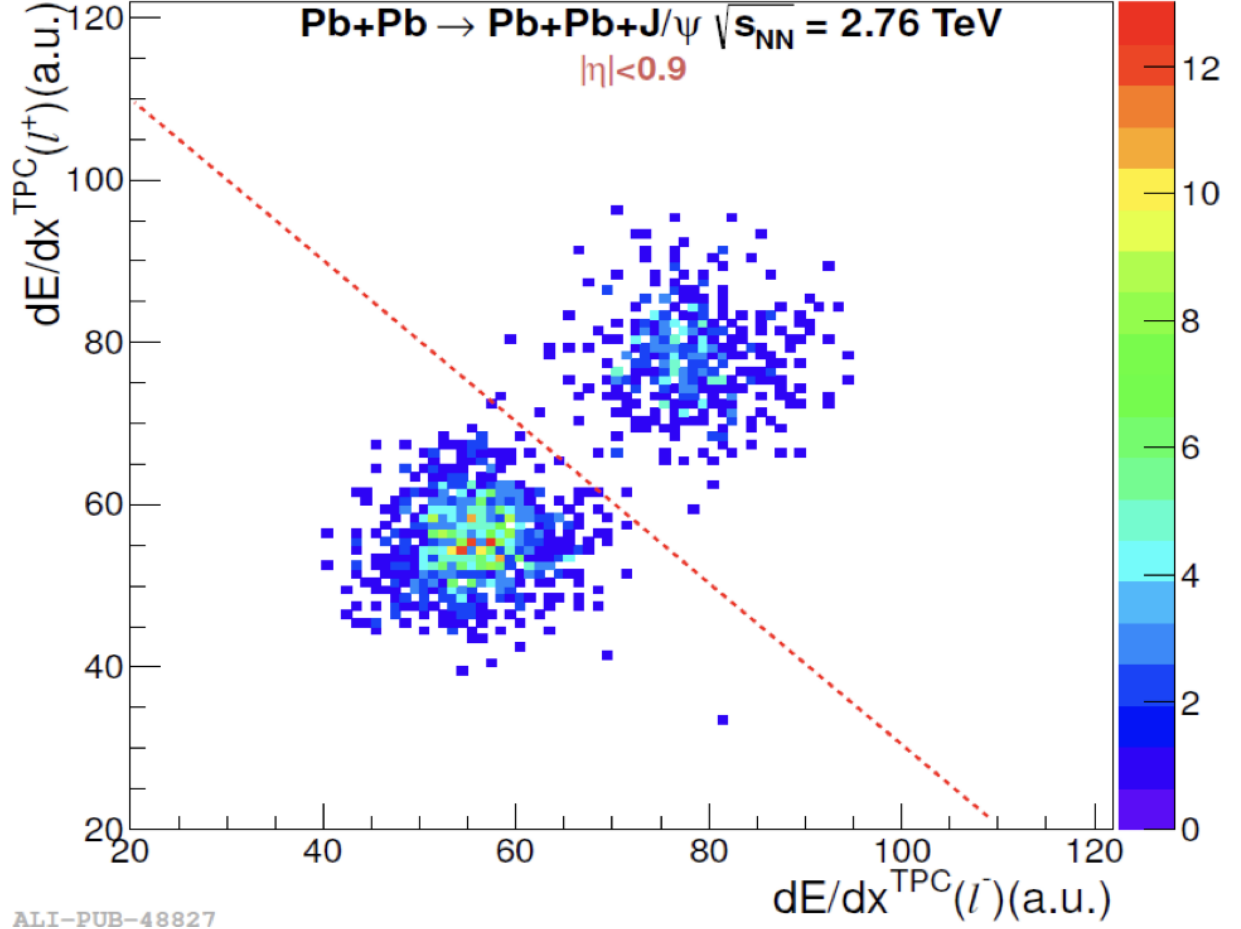
Figure 1.1: Separation of electrons (left) and muons (right) in the TPC; back-to-back decay from the J/ψ meson from Run 1 [7].

make a statement about whether the energies of the photons are sufficiently low for Low's theorem to hold [6][4]. This thesis is structured as follows:

Section 2 introduces Low's theorem and motivates the usage of ultra-peripheral collisions along with the J/ψ meson. In Sec. 3 the updated LHC and ALICE setups are discussed, and the necessary detector parts for the observation are shortly examined. The current detector system works in $|\eta| < 1$ direction, thus restricting the measurement to the mid-rapidity region. Section 4 focuses on the different possibilities of interactions leading to photon detection since the emitted photons are detected by their conversion into electron-positron pairs in the detector material. In Sec. 5 the introduction and analysis of the model calculations are given in detail. Finally, in Sec. 6 a conclusion and outlook are presented.

Section 2

Low's Theorem and Experimental Approach

2.1   Low's theorem

In the late 1950s, F. Low proposed that the first two terms of the differential inner bremsstrahlung cross-section may be calculated exactly, and thus the cross-section in k_T powers can be understood with [1]

$$\sigma = \frac{\sigma_0}{k} + \sigma_1 + k\sigma_2 + \dots .$$ (2.1)

The inner bremsstrahlung yield can be calculated from the non-radiative amplitudes of the original process by summing over all charged particles included in the collision. The interaction of two incoming and two outgoing particles was considered for the calculation $p_1+p_2 \rightarrow p_3+p_4+k$, where p_i represents a hadron with its corresponding four-momentum, and k a photon and its momentum. The affiliated amplitude M for a produced photon with polarization ϵ is [8]

$$M\left(p_1 p_2 ; p_3 p_4 k\right) = M_0\left(p_1 p_2 ; p_3 p_4\right) \left(\frac{e_1 p_1 \cdot \varepsilon}{\left(p_1 - k\right)^2} + \frac{e_3 p_3 \cdot \varepsilon}{\left(p_3 + k\right)^2} \right)$$ (2.2)

$$= M_0\left(p_1 p_2 ; p_3 p_4\right) \left(\sum_i \frac{\eta_i e_i p_i \cdot \epsilon}{2 p_i \cdot k} \right),$$ (2.3)

where e_i is the charge of the particle p_i and η_i is either +1 or -1 for an outgoing or incoming hadron, respectively. The following assumptions were made to obtain the formula

$$M_0\left(p_1 - kp_2 ; p_3 p_4\right) \sim M_0\left(p_1 p_2 ; p_3 + kp_4\right) \sim M_0\left(p_1 p_2 ; p_3 p_4\right).$$ (2.4)
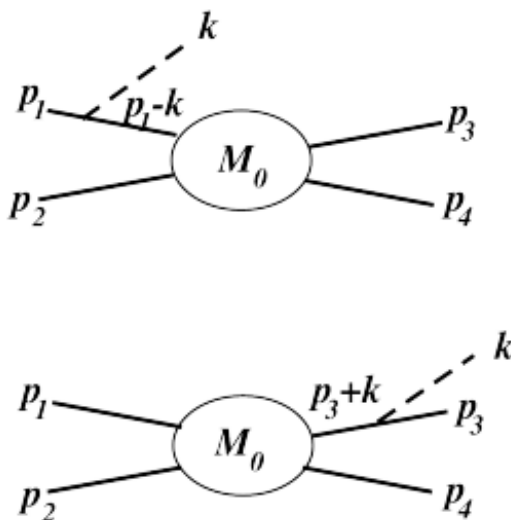
Figure 2.1: Feynman diagrams for the $p_1 + p_2 \rightarrow p_3 + p_4 + k$ process [8].

In high energy physics, $|\mathbf{p_1}|$ and $|\mathbf{p_3}|$ are usually much greater than the photon transverse momentum, in the C.M. (center of mass) frame, which leads to the insight that the amplitude M_0 is approximately independent of k [8].

The process can thus be generalized for N outgoing particles. This leads to an amplitude of

$$M\left(p_1 p_2 ; p_3 p_4 \ldots p_N k\right) = M_0\left(p_1 p_2 ; p_3 p_4 \ldots p_N\right)\left(\sum_i \frac{\eta_i e_i p_i \cdot \varepsilon}{2 p_i \cdot k}\right). \tag{2.5}$$

Considering the relation between cross-sections and Feynman amplitudes [1] eq. 2.5 gives

$$\frac{dN_\gamma}{d^3 k} = \frac{\alpha}{(2\pi)^2 k_0} \int d^3 p_1 d^3 p_2 d^3 p_3 \ldots d^3 p_N \sum_{i,j=1}^N \eta_i \eta_j e_i e_j \frac{-\left(p_i \cdot p_j\right)}{\left(p_i \cdot k\right)\left(p_j \cdot k\right)} \frac{dN_{\text{hadrons}}}{d^3 p_1 d^3 p_2 d^3 p_3 \ldots d^3 p_N} \tag{2.6}$$

which breaks down to

$$\frac{d^3 \mathrm{N}_\gamma}{d|\mathbf{k}|d\eta d\phi} = -\frac{2\alpha}{(2\pi)^2} \cos(\vartheta/2) \sin(\vartheta/2) E_\gamma \sin\vartheta \left(\sum_{\text{Particle } i} \frac{\eta_i e_i P_{\mathbf{i}}}{P_{\mathbf{i}} \mathrm{K}}\right)^2 \sim \frac{1}{E_\gamma}. \tag{2.7}$$

Here ϑ represents the polar angle and ϕ the azimuth angle of the photon in detector coordinates for a single event. The bremsstrahlung spectrum follows the typical $1/E_\gamma$ divergence.

Anomalous soft photon production

Low's theorem is of interest in regard to the anomalous soft photon production in hadron production. In some measurements that began in the 1980s, the soft photon production with hadrons in the final state is by a factor of 4 greater than expected from the theorem introduced by Low [1] [8]. In evaluations considering the $e^+ e^- \rightarrow Z \rightarrow \mu^+ \mu^-$ on the other hand, no excess was observed. This excess photon yield with low transverse momentum is commonly referred to as anomalous soft photon yield. A list of the experimental assessments of Low's theorem is presented in Table 2.1.

Experiment	Collision Energy	Photon k_T	Photon/Brem Ratio
K^+p, CERN,WA27, BEBC (1984)	70GeV/c	$k_T < 60$MeV/c	4.0 ± 0.8
K^+p, CERN,NA22, EHS (1993)	250GeV/c	$k_T < 40$MeV/c	6.4 ± 1.6
π^+p, CERN,NA22, EHS (1997)	250GeV/c	$k_T < 40$MeV/c	6.9 ± 1.3
π^-p, CERN,WA83,OMEGA (1997)	280GeV/c	$k_T < 10$MeV/c	7.9 ± 1.4
π^+p, CERN,WA91,OMEGA (2002)	280GeV/c	$k_T < 20$MeV/c	5.3 ± 0.9
pp, CERN, WA102, OMEGA (2002)	450GeV/c	$k_T < 20$MeV/c	4.1 ± 0.8
$e^+e^- \to$ hadrons, CERN, DELPHI with hadron production (2010)	~ 91GeV(CM)	$k_T < 60$MeV/c	4.0
$e^+e^- \to \mu^+\mu$ with no hadron production (2008)	~ 91GeV(CM)	$k_T < 60$MeV/c	1.0

Table 2.1: The ratio of the soft photon yield associated with hadron production to the bremsstrahlung yield [8].

Experimental assessment

Experimental data leads to the assumption that anomalous soft photons (ASP) are only present when a hadron is produced in the final state. This was shown by the DELPHI collaboration. They compared the yield in Z^0-decay and the corresponding $e^+ + e^- \to \mu^+\mu^-$ reaction [9], [10]. The DELPHI collaboration found that the ASP yield increases linearly with the number of either charged or neutral particles originating in the same process, but increases faster with the neutral particle multiplicity than the charged one.
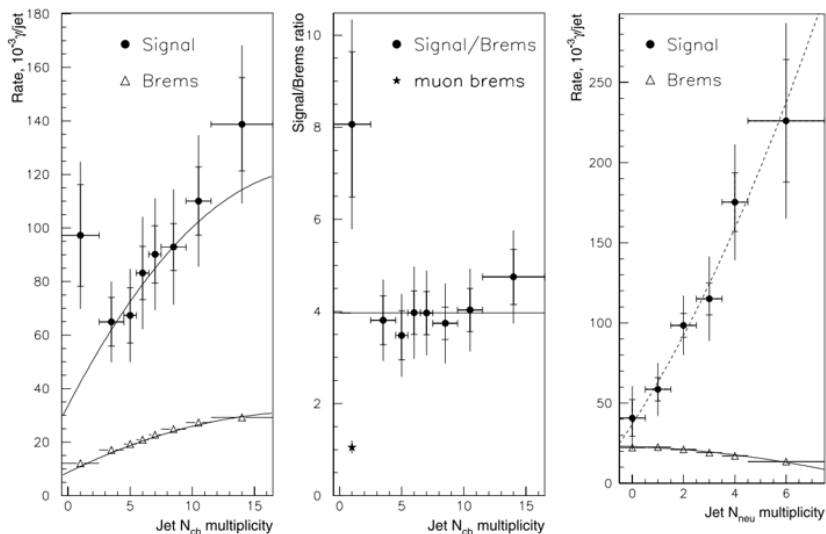

Figure 2.2: Anomalous soft photon yield examined by the DELPHI collaboration in 2010 [9].

Theoretical approach to ASP

Many different models are trying to explain the effect of anomalous soft photon production in QCD hadron production processes. Since for a fully theoretical approach, QCD and QED effects have to be considered, a complete model is not yet established. The models vary from a form of the cold quark-gluon system being the source of these low photons [11], where these are being produced in either $q + \bar{q} \to \gamma + g$ or $q + g \to \gamma + q$, to the concept of parton trajectories following string breaking in string fragmentation [12].

To summarize, neither experimental data nor theoretical calculations can explain the occurrence of anomalous soft photon production in hadronic QCD production.

2.2 Ultra Peripheral Collisions

At the end of the last century, the theory from Enrico Fermi "On the Theory of Collisions Between Atoms and Elastically Charged Particles" [13] became more popular among scientists working on colliding physics since it opened up a window to discover new physics in the collision of nuclei.

In the publication, Fermi treated the electromagnetic field of a charged particle as a flux of virtual photons. In 1934 Weizsäcker and Williams included ultra-relativistic particles in Fermi's approach, which is known as the *Weizsäcker and Williams method* [14].

Two electromagnetic processes can occur; a photon from one ion strikes the other one, or photons that are emitted by each of the nuclei collide with each other in a photon-photon-like collision. Both of them are shortly introduced. The focus lies on the interaction involving the production of $J/\psi's$.

The cross-section σ_X for the required photoproduction is

$$\sigma_X = \int d\omega \frac{n(\omega)}{\omega} \sigma_X^\gamma(\omega), \tag{2.8}$$

$\sigma_X^\gamma(\omega)$ as the photonuclear cross-section and $n(\omega)$ as the number of photons with the energy ω. For two-photon processes the cross-section reads as follows:

$$\sigma_X = \int d\omega_1 d\omega_2 \frac{n(\omega_1)}{\omega_1} \frac{n(\omega_2)}{\omega_2} \sigma_X^{\gamma\gamma}(\omega_1, \omega_2), \tag{2.9}$$

where $\sigma_X^{\gamma\gamma}(\omega_1, \omega_2)$ is the two-photon cross-section [15].

Since electromagnetic interactions are not the only ones occurring in these kinds of collisions, Fermi's theory has been extended to strong interactions between nuclei in ultra-peripheral collisions. While many improvements in the field have been published since the beginning of 1924, especially the introduction to relativistic heavy-ion accelerators is of particular interest for this thesis.

For further calculations, the knowledge about the photon flux originating in ion-ion separations is important. The interaction time of the nuclei is

$$\Delta t \sim \frac{b}{\gamma v} \tag{2.10}$$

$$\hookrightarrow \omega^{max} = \frac{\hbar}{\Delta t} \sim \frac{\gamma \hbar v}{b} \tag{2.11}$$

b represents the impact parameter and ω^{max} the maximum photon energy emerging. For a collision where the two ions barely touch, we can consider $b_{min} = 2R_A$, where R_A is the radius of the nucleus. For the collision generator, a precise measurement for the radius of the nuclei is implemented by accessing the value from the Particle Data Group (PDG).

Due to the fact that the final state multiplicity is much smaller in ultra-peripheral collisions (UPCs) and the possible full reconstruction of it, the topology differs substantially from conventional hadronic interactions. With the photon p_T being rather small, the final state p_T is also of smaller values, which leads to an extremely clean experimental signature for the J/ψ decay.

Photoproduction at Hadron Colliders

Photoproduction at hadron colliders is significant due to its sensitivity to the gluon distribution in nucleons and nuclei. However, here we are focusing on the production of heavy vector mesons in this kind of interaction.

Due to the photon holding the quantum numbers $J^{PC} = 1^{--}$, vector meson production is preferred. This leads to the dominant production of vector mesons at interactions resulting in a hadronic final state

$$A + A \rightarrow A + A + V.$$

A photon from the electromagnetic field of one projectile interacts with the field of the other one, resulting in vector meson production. The production of vector mesons has been studied since the 1960s which results in a vast knowledge of how to calculate such an interaction.
The cross-section can be obtained including the aid of eq. 2.8. By varying the variable from the photon-energy ω to the pseudorapidity y:

$$\frac{d\sigma(A + A \rightarrow A + A + V)}{dy} = n(\omega)\sigma_{\gamma A \rightarrow VA}(\omega), \qquad (2.12)$$

where $\omega = (M_V c^2/2)exp(y)$ and M_V represents the mass of the vector meson in question. The colliding nuclei A remain unexcited after the collision, which induces the dominant contribution to the total cross-section. The excitation of the nuclei A is possible and contributes around ten percent to the total cross-section. It is possible to experimentally differentiate between these two processes with a zero-degree calorimeter since the excited nuclei emit a neutron in beam direction, which can be detected inside of it.
With known photon flux the differential cross-section can be received by directly measuring the vector meson cross-section for a given photon energy.
The uncertainty principle has an influence on the lifetime and can thus be calculated for a photon of virtuality Q by

$$\Delta t \approx \frac{\hbar}{\sqrt{M_V^2 c^4 + Q^2 c^2}} \approx \frac{1}{M_V c^2}. \qquad (2.13)$$

Since photons have low virtuality at hadron colliders the last approximation holds.

<div align="center">

Meson Au+Au, RHIC Pb + Pb, LHC

	σ(mb)	σ (mb)
ρ^0	590	5200
ω	59	490
ϕ	39	460
J/ψ	0.29	32

</div>

Table 2.2: Cross-section for exclusive vector meson production in Au+Au and Pb+Pb interactions at RHIC and the LHC, with $\sqrt{s_{RHIC}}=$ 100GeV and $\sqrt{s_{LHC}}=$ 2.76TeV [15].

For the cross-sections written in Tab. 2.2 proton targets were used to calculate the total cross-section $\sigma_{tot}(VA)$. Gluon shadowing may reduce the cross-section for heavy vector mesons, like the J/ψ [16].
Quantum mechanical interference makes it impossible to determine which of the nuclei acts as the

target and which one as the projectile [17]. The interference of both cross-sections is calculated by adding the amplitudes A_1 and A_2 [15]:

$$\frac{\hbar d\sigma}{dy dp_T} = \int_{b>2R} |A_1 \pm A_2|^2 d^2 b \tag{2.14}$$

Symmetry requires that $A_1 = A_2$, if the interference is maximal. The effect of the interference is destructive due to the negative parity of vector mesons and thus affects the dip in the mid-rapidity of the differential cross-section. When the vector meson is treated as a plane wave, the sum becomes

$$|A_1 \pm A_2|^2 = 2A_0^2\left(1 \pm cos(\frac{p \cdot b}{\hbar})\right) \tag{2.15}$$

at mid-rapidity [15]. For vector meson production the two amplitudes are subtracted from each other, due to the negative parity of the vector meson. For $p_T \to 0$ emission disappears in ion-ion collisions and doubles for $p\bar{p}$ experiments.

Away from mid-rapidity, $|A_1| \neq |A_2|$, both the photon flux and photonuclear cross-sections will differ. The vector mesons of interest are in the mid-rapidity range, which is the reason further discussion will be unheeded.

2.3   The J/ψ meson

At the end of 1974 the groups of Burton Richter and Samuel C. C. Ting, at different locations, found something unexpected. A peak in the $e^+e^- \to hadrons$ cross-section and the mass spectrum of hadrons decaying into e^+e^- and $\mu^+\mu^-$ was detected. The group of Richter worked at the Stanford Linear Accelerator (SLAC) and found a peak in their data with the energy of $E = 3.105 \pm 0.003$GeV and an upper limit of $\Gamma \leq 1.3$MeV for the full width at half maximum (FWHM). Because of the shape, the paths of the daughter particles have made, its name was proposed as Ψ. The Ting group at Brookhaven National Laboratory's alternating gradient synchrotron named the particle, responsible for the mass peak at $m = 3.1$GeV, J [18] [19].

Due to the timely discovery of the meson, it is nowadays called J/ψ which Ting and Richter were awarded the Nobel Prize in 1976 [20].

The discovery led to the realization that the theory of the charm quark c is part of reality. Charmonium is a $c\bar{c}$ state with a mass of $m = 3096.900 \pm 0.006$MeV and a decay width $\Gamma = 92.7 \pm 1.7$keV. The J/ψ quarkonium decays mainly in a hadronic channel $(87.7 \pm 0.5)\%$, an e^+e^- pair $(5.971 \pm 0.032)\%$ and a $\mu^+\mu^-$ pair $(5.961 \pm 0.033)\%$. Due to the quantum numbers, $J^{PC} = 1^{--}$, the meson decays rather slowly, compared to other quarkoniums [23] [24].
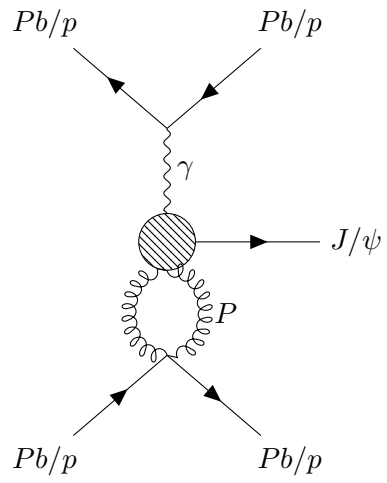
Figure 2.3: The Feynman Diagram for the J/ψ production in UPCs.

Section 3

The Large Hadron Collider and ALICE

The European Organization for Nuclear Research (CERN) provides the ideal environment to measure and perform experiments focusing on particle and nuclear physics. The Large Hadron Collider's (LHC) main collider is the world's largest particle accelerator with a circumference of 27km. The accelerator was designed to achieve center of mass energies of up to $\sqrt{s} = 14$TeV for pp- and $\sqrt{s_{NN}} = 5.5$TeV for Pb-Pb collisions, with a peak luminosity of $\mathcal{L} = 10^{34}$ cm^{-2}s^{-1} and $\mathcal{L} = 10^{27}$cm^{-2} s^{-1} respectively [2]. In order to accelerate the particles to their desired energies, they have to pass different pre-accelerators, with each increasing the energy before passing the particles into the next one.

For further development, the operation stopped in 2018 for three years, known as Long Shutdown 2 (LS2), where major upgrades and maintenance were performed on the instruments. The interaction points used this opportunity to upgrade their components as well.
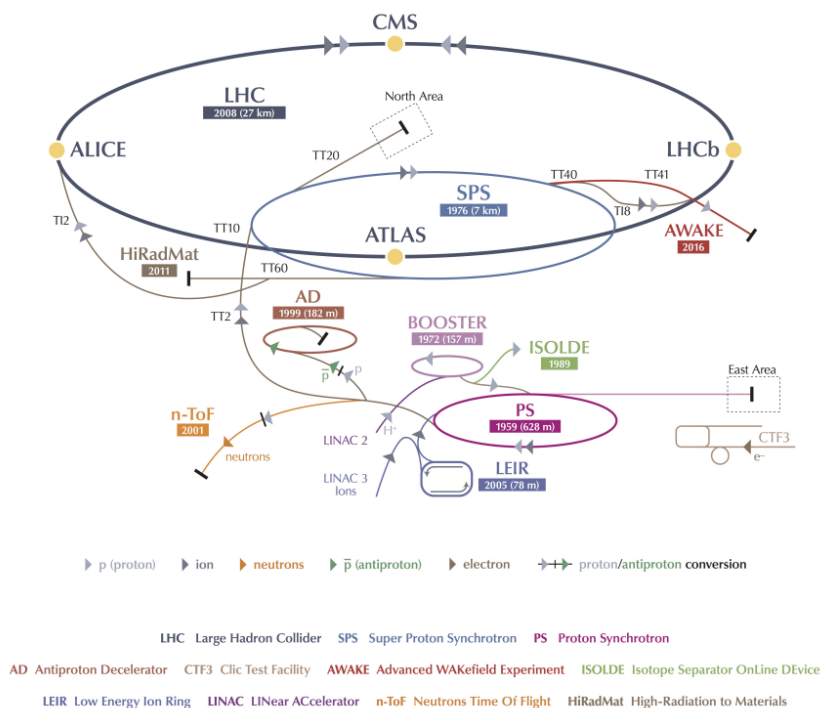

Figure 3.1: CERN accelerator complex [25].

The ALICE collaboration

The ALICE experiment (A Large Ion Collider Experiment) is designed to study heavy-ion collisions of the four big experiments at the LHC. Because of its advanced measuring capability, it is possible to study a vast amount of rare events at ALICE, for which the components of the detector have to be steadily improved. To obtain results faster, the collision rate was increased to 50kHz for collisions of heavy ions. The ALICE experiment was upgraded with continuous readout to a $Pb - Pb$ interaction rate of 50kHz during LS2 and will be completely changed during LS4 for the new ALICE 3 in 2032 to achieve even higher collision rates. The experiment is the ideal place to advance (ultra) soft-photon studies in QCD and QED using UPCs. The necessary detectors for the specific observation are briefly described below.
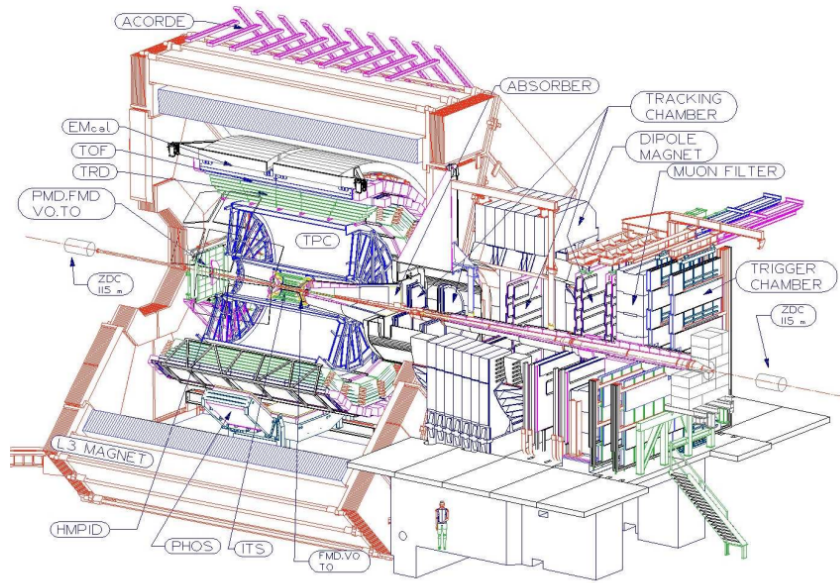

Figure 3.2: sketch of the Alice detector [2].

The Inner Tracking System

The inner tracking system has the task of tracking charged particles close to the interaction vertex, it was upgraded to the ITS2 during LS2.
The ITS2 was developed to increase the readout rate up to 100kHz for Pb-Pb collisions and 400kHz for pp-collisions with a corresponding upgrade for the geometry and electronic network system regarding such high statistics. It contains seven layers of silicon pixel detectors. The inner barrel is made of three layers starting at a vertex distance of 22.4mm, which consists of Silicon Pixel Detectors (SPD). Due to the downsizing of the inner barrel, the beampipe had to be reduced at the same time, resulting in an inner radius of 19.2mm [26].
The outer barrel is made of the middle and outer layers consisting of two layers [26].
During LS2 10m^2 of the CMOS (Complementary Metal-Oxide Semiconductor) Monolithic Active Pixel Sensors (MAPS) were installed. This resulted in a reduction of the silicon material budget by a factor of seven compared to the ITS used before. Combining all the new elements, it was possible to reduce the material budget of the inner layer to 0.3% and of the outer layer to 0.81%. The new chip has a detection efficiency of a minimum of 99% with a fake hit rate of 10^{-5}, which is possible due to the size of a one-pixel chip of 15mm $\times$30mm.
With a lot more improvements done for only the ITS, the ITS 2 detector can cover a pseudora-

pidity range of $|\eta| < 1$. The future inner tracking system for ALICE 3 in 2032 will cover a range of $|\eta| < 4$ [2].

Time Projection Chamber

The time projection chamber (TPC) together with the ITS make up the core of charged particle identification at ALICE. With the ITS being responsible for high spatial-resolution tracking, the TPC is in charge of tracking and identifying the particles. The TPC is a 5m long hollow cylindrical barrel. It has an inner radius of 0.8m and an outer one of about 2.5m. The TPC is filled with $90m^3$ of counting gas [5]. The composition in use is Ne-CO_2-N_2 (90:10:5) [5].
The charged particles ionize the gas and leave a trace of electrons along their trajectory, which are then accelerated by the homogeneous electric field toward the read-out modules.
The electrically charged particles inside the TPC are characterized by the energy loss per unit length dE/dx and depends on the charge, the particle's velocity, and the medium's physical properties. This is described by the Bethe-Bloch formula [27]. When expressing the energy loss in terms of the particle's momentum, $p = \beta\gamma \cdot m$, the traversing particles can be distinguished by their physical properties.
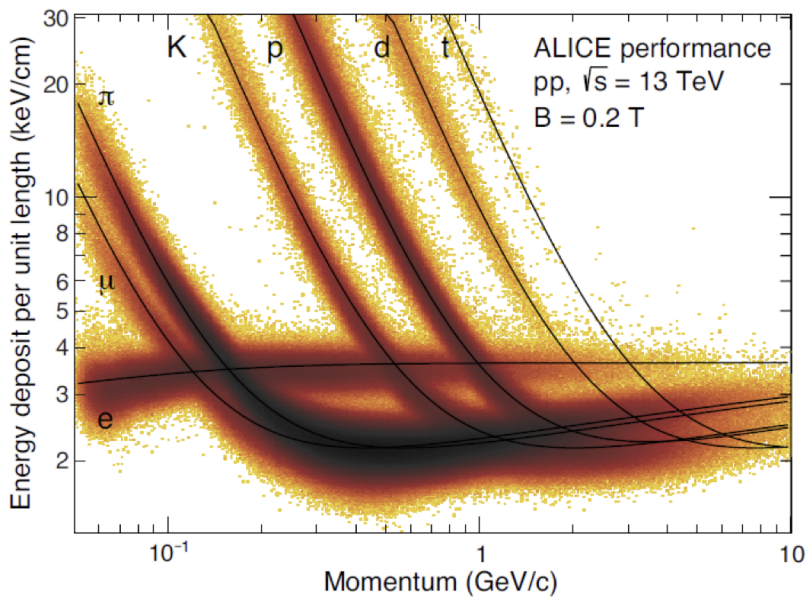

Figure 3.3: Example of the particle identification of the TPC; electrons and muons can be easily separated from each other [28].

Time of Flight

The time of flight detector (TOF) provides coverage of $|\eta| < 0.9$. As the inner tracking system, the TOF consists of an inner and outer barrel. The TOF achieves a time resolution of 56ps r.m.s with a low material budget of $1 - 3\%$. It can distinguish particles with large mass differences by comparing the arrival time with a computed estimation for it. The current setup has a detector efficiency of $\sim 98 - 99\%$ [29].
For the upcoming ALICE 3 experiment the TOF detector will be upgraded to cover a range of $|\eta| < 4$ and a time resolution of up to 20ps [2].

Zero Degree Calorimeter

The zero-degree calorimeter (ZDC) was established for two purposes: The first is to measure the centrality of an interaction process and the second to measure the delivered luminosity of the experiment by exploiting neutron emission from electromagnetic dissociation processes. The measurement of neutrons from the de-excitation processes of the nuclei is of interest for the measurements of this thesis.

The ZDC contains three sampling calorimeters 112.5m away from the interaction point [30]. The LHC dipole separates the outgoing beam from the spectator particles, covering a pseudo-rapidity range of $4.8 < \eta < 5.7$ and allows the separation between hadronic and electromagnetic interactions. For the performance boost for RUN 3 and 4 at the LHC, the ZDC calorimeter is extended with a continuous readout system, which helps to separate between coherent and incoherent vector-meson production at UPC interactions [30].

Section 4

Interactions of Photons with Matter

In this section, we will shortly discuss the interactions of photons arising within the detector material. A photon γ cannot be detected directly, which is why detectors have to rely on their interactions with matter. The three most common processes are Compton scattering, the photoelectric effect, and pair conversion.

Compton effect

The Compton effect describes an inelastic scattering of the photon off a particle. The photon collides with the particle and passes on a part of its energy, which could accelerate it. With momentum and energy conservation the interaction particle cannot absorb the whole photon. For high energies ($E_\gamma >> m_e c^2$) the cross-section of the Compton scattering follows

$$\sigma_C \propto Z/E_\gamma. \tag{4.1}$$

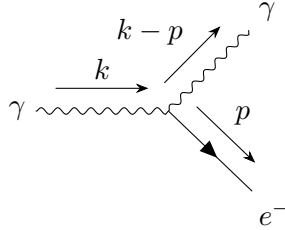This assumption can be made concerning the photon energies considered in this work [31].

Figure 4.1: Feynman diagram for Compton scattering, with k as the photon momentum and p the particle momentum.

Photoelectric effect

The Photoelectric effect is the absorption of a photon with energy $h \cdot \nu > E_b$ by an electron from one of the atomic shells. It is then re-emissioned with an energy $E_{kin} = h \cdot nu - E_b$, ν as the initial photon frequency, h the Planck constant and E_b the binding energy of the electron.
Only if the atom absorbs some of the initial photon momentum (recoiling), energy and momentum conservation can be met. The total cross-section for the photo-effect is the sum of all Z-shell electrons in the K-shell. For high γ energies ($E_\gamma >> E_b(K)$) the cross-section flattens from

$$\sigma_{ph} \propto Z^5 \left(\frac{m_e c^2}{E_\gamma} \right)^{7/2} \tag{4.2}$$

for rather low photon energies to [31]

$$\sigma_{ph} \sim Z^5/E_\gamma. \tag{4.3}$$

Pair conversion

The third possibility of a photon interacting with matter is pair conversion. It occurs for higher energetic photons with an energy

$$E_\gamma > 2 \cdot m_e c^2, \tag{4.4}$$

m_e representing the electron mass and c the speed of light. If the energy of the γ is sufficiently large, it can produce an electron-positron pair when the field of an atomic nucleus is present. The differential cross-section of pair conversion is given by $x = E/k$ (E electron-/positron-energy, k photon-energy) by:

$$\frac{d\sigma}{dx} = \frac{A}{X_0 N_A} \left[1 - \frac{4}{3} \cdot x(1-x) \right]. \tag{4.5}$$

A represents the atomic number, X_0 the radiation length multiplied with the density of the material and N_A the Avogadro number.
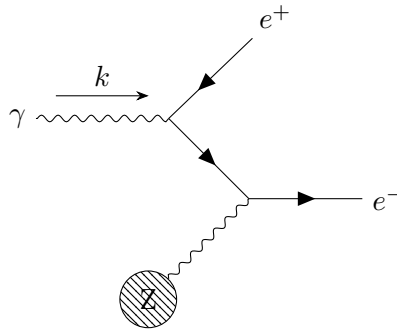

Figure 4.2: Feynman diagram for pair production.

The integrated cross-section for high energies is [32]

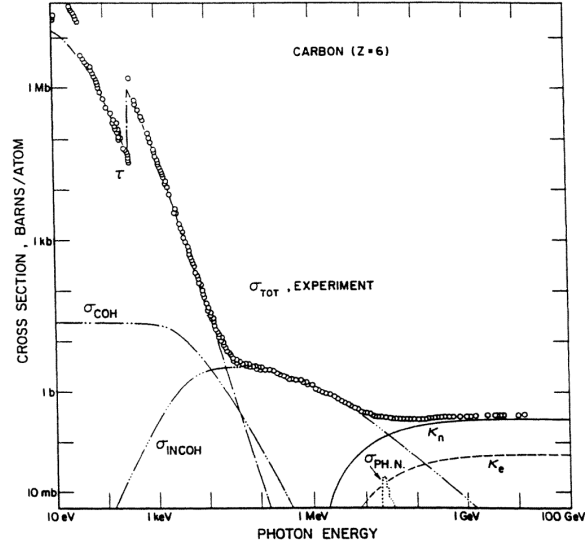$$\sigma = \frac{7}{9} \left(\frac{A}{X_0 N_A} \right). \tag{4.6}$$

Figure 4.3: Contributions of atomic photo-effect τ, coherent scattering σ_{COH}, incoherent (Compton) scattering σ_{INCOH}, nuclear-field pair production κ_n, electron-field pair production (triplet) κ_e, and nuclear photo absorption $\sigma_{PH.N}$ to the total measured cross section σ_{TOT} (circles) in carbon over the photon energy range 10 eV to 100 GeV [33].

Section 5

Model Calculations

In this thesis, the inner bremsstrahlung of the following two decay channels of the J/ψ meson is studied, $J/\psi \to e^+e^-$ and $J/\psi \to \mu^+\mu^-$. The analysis is discussed in detail with the example of ultraperipheral Pb-Pb collisions. Other collision systems, including ALICE 3 applications [2], are given in the later part of this section. The evaluation follows the decay channel simulated by "STARlight" [34].

As mentioned before this thesis uses the $A + A \to J/\psi(\to l^+l^-)$ event generated by STARlight, as a test of Low's theorem for soft photons for possible ALICE measurements. In this work, the cross-section for the emission of bremsstrahlung photons is calculated. The cross-section for the J/ψ is done by STARlight's calculation for UPCs. Here Pb-Pb collisions are examined in the "STARlight" data. Other collision systems are calculated as well.

5.1 "STARlight"

Ultra-peripheral collisions (UPCs) became a significant source of study at the LHC in the last two decades. Since the interactions at UPCs are either photonuclear or two-photonic, "STARlight" was introduced to compute and calculate the cross-section of specific processes via Monte-Carlo simulations. We are only interested in the simulation of J/ψ's and will thus only briefly discuss the physical calculations the program does to compute them.

For the calculation of the cross-section, the form factor of the nuclei is of great importance.

For heavy nuclei, "STARlight" either uses measured parameters for the nuclear radius [36] or the following Woods-Saxon parameterization:

$$R_A = 1.2\text{fm} \cdot A^{1/3}. \tag{5.1}$$

Each beam energy corresponds to its Lorentz factor γ with

$$\gamma = E_{beam}/m_{proton}. \tag{5.2}$$

The photon number density [35], at photon energy k and impact parameter b, follows

$$N(k,b) = \frac{Z^2\alpha \cdot k}{\pi^2(\hbar c)^2} \frac{1}{\gamma^2} \left[K_1^1(x) + \frac{1}{\gamma^2} \cdot K_2^2(x) \right], \tag{5.3}$$

with $x = kb/\gamma\hbar c$, α the electromagnetic fine structure constant and K_0, K_1 the modified Bessel functions. Further calculations are carried out with the photon number density at the core. Photonuclear interaction produces vector mesons between the particles at UPCs, the focus lies

on this type of interaction, leaving out further considerations of two-photon interactions [15]. Assuming that the beams do not interact with each other, the photon flux is given by

$$\frac{dN_\gamma(k)}{dk} = \int d^2b P_{NOHAD}(\vec{b}) N(k, \vec{b}),$$ (5.4)

with again the photon energy k and at position $\vec{b}$ of the nucleus. The probability P_{NOHAD} of not having a hadronic interaction, must be implemented in different ways for different types of collision. In particular, for nucleus-nucleus collisions it looks as follows:

$$P_{NOHAD}(\vec{b}) = e^{-\sigma_{NN} T_{AA}(\vec{b})}.$$ (5.5)

Here $T_{AA}(\vec{b})$ represents the nuclear overlap function which can be computed from the density profiles with the density following a Woods-Saxon distribution, the cross-section the parameterization of the PDG for pp-collisions with a center of mass energy above 7GeV results in [38]

$$\sigma = \left(33.73 + 0.2838 \ln^2(r) + 13.67 r^{-0.412} - 7.77 r^{-0.5626}\right) \text{mb},$$ (5.6)

$$r = s/1\text{GeV}^2.$$ (5.7)

The probability $P_{NOHAD}(\vec{b})$ reduces the $\gamma\gamma$ luminosity by up to 20%, since there is still a probability that the two nuclei will interact at impact parameters larger than $2R_A$ [37]. For different types of photonuclear reactions, there exist different types of calculations which have to be performed in order to get an accurate tree of data. Since the cross-sections are mostly based on HERA parametrizations of $\gamma p \to V p$ data, the cross-section for the J/ψ meson is calculated using the following formula

$$\sigma(\gamma + p \to V + p) = \sigma_P \cdot \left[1 - \frac{(m_p + m_V)^2}{W_{\gamma p}^2}\right]^2 \cdot W_{\gamma p}^\epsilon.$$ (5.8)

The values for σ_P and ϵ are obtained from [34]. The cross-section is parameterized by the γp center of mass energy $W_{\gamma p}$, m_V replaced by the respective mass of the final state, in this case, of the J/ψ meson.

With the desired meson production belonging to the class of incoherent vector meson production, the cross-section is calculated under the assumption that it does scale the same way as the total inelastic cross-section for the vector meson:

$$\frac{\sigma_{inc}(\gamma + A \to V + A*)}{\sigma(\gamma + p \to V + p)} = \frac{\sigma_{inel}(A + V)}{\sigma_{inel}(p + V)}.$$ (5.9)

Assuming further that the total inelastic cross-section can be expressed as [34]

$$\sigma_{\text{inc}}(\gamma + A \to V + A) = \frac{4\pi\alpha}{f_v^2} \int \left(1 - e^{-\sigma_{VN} T(b)}\right) db^2.$$ (5.10)

The term in parentheses represents the probability of having a minimum of one vector-meson-nucleon interaction at the impact parameter b. Because the form factor is needed for the calculation, the data has confirmed the usage of

$$F(Q^2) = e^{-bQ^2}$$ (5.11)

as the form-factor for heavier vector-mesons, with $b = 4.0\text{GeV}^{-2}$ for the J/ψ [39]. The p_T spectrum can be generated assuming that photoproduction is independent of the nuclei [34].
The first phase of the STARlight process is the calculation of the cross-section and other kinematics needed for the simulations. These values are stored in a series of tables. The first tables

created are for the event mass, the rapidity, and $d^2N/dY\,dW$. For photonuclear vector meson production, the mass distribution follows a Breit-Wigner distribution, the parameterization taken from the PDG. Additionally, the second table of information regarding the transverse momentum is created. After the first phase, the program uses the look-up tables created before to simulate nuclear interactions. As the result, "STARlight" can generate a vast amount of events in a comparatively short time.

The simulation is run as a single job, with a total of one million events. This "STARlight" simulation needs about half an hour to finish. The run time and simulation are done for the two decay channels independently from each other. The analysis and further usage of the generated data are facilitated, since "STARlight" stores the data on an event-by-event basis. This means that every dilepton is stored at the same number with its respective partner. The data points are saved in a TTree format for additional purposes.

The grid was filled inserting the formula for single events since "STARlight" assures that the J/ψ only decays to either a muon- or an electron pair.

The following settings are used for the simulations:

variable	setting
collision Energy	5.5 TeV for Pb-Pb
	13 TeV for pp
	7 TeV for OO
	6.46 TeV for KrKr
Beam_1_Energy	$\sqrt{\left(\frac{Z_1}{A_1} \cdot \frac{A_2}{Z_2} \cdot E/2\right)}$
Beam_2_Energy	$\sqrt{\left(\frac{A_1}{Z_1} \cdot \frac{Z_2}{A_2} \cdot E/2\right)}$
Gamma_1	2.93092 TeV
Gamma_2	2.93092 TeV
W_N_Bins	5000
Rap_N_Bins	40
Rap_Max	7.05
N_Events	10Mil
Prod_Pid	443013 for $\mu^-\mu^+-$decay
Prod_Pid	443011 for e^-e^+-decay

Table 5.1: "STARlight" settings.

STARlight analysis

The relativistic velocity of a particle is given by

$$\beta = |\vec{p}|/E. \tag{5.12}$$

Due to the produced J/ψ being nearly at rest, the assumption can be made that the lepton pair originating from the decay essentially orientated back to back. The case of an extremely high energy photon is neglected for the time being. This can be seen in its distribution of the transverse momentum. Following the assumption that the leptons are emitted back to back, the transverse momenta, as well as their energies, are calculated regarding energy and momentum conservation.

$$\vec{p}_{\bar{l}} = -\vec{p}_l =: \vec{p} \tag{5.13}$$

In the following calculations, M and P are the mass and the 4-momentum of the J/ψ and m_l and P_l, $P_{\bar{l}}$ are the mass and 4-momentum of the lepton and anti-lepton, respectively.
Following the relation, $P \cdot P_l = ME_l$, an expression for the absolute value of the three momenta of the (anti) lepton is obtained via

$$|\vec{p}| = \sqrt{E_l^2 - m_l^2} = \frac{1}{2M} \cdot \sqrt{\left((M-m)^2 - m^2\right) \cdot \left((M+m)^2 - m^2\right)}. \tag{5.14}$$

The expression simplifies to

$$|\vec{p}| = \frac{M}{2} \cdot \sqrt{1 - 2\frac{m^2}{M^2}} \; . \tag{5.15}$$

Inserting the electron and muon mass into the equation the absolute value of the momentum is:

$$|\vec{p}_\mu| \approx 1.547\,\text{GeV/c}$$
$$|\vec{p}_e| \approx 1.548\,\text{GeV/c}$$

For the case of a J/ψ decay at rest, the velocities of the leptons are calculated with $\beta = p/E$:

$$\beta_{e^-} \approx 1 \tag{5.16}$$
$$\beta_{\mu^-} \approx 0.9974 \tag{5.17}$$

For the masses, the values from the PDG are used [41]. To compare the simulations, two approaches are made: the first with the p_T distribution from the leptons and the second with the invariant masses are inserted into eq. 5.15. The p_T and mass distributions are received by the TLorentzVector Class from root. For the masses "STARlight" computes:

$$m_{J/\psi} = (3.097 \pm 1.12 \cdot 10^{-4})\text{GeV}$$
$$m_{\mu^\pm} = (0.1057 \pm 8.6 \cdot 10^{-8})\text{GeV}$$
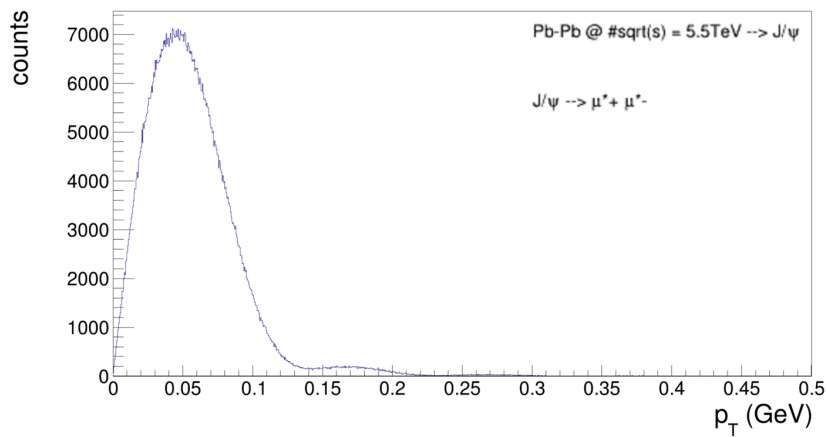$$m_{e^\pm} = (5.44 \pm 1.73) \cdot 10^{-4}\text{GeV}$$

The invariant mass figures can be observed in fig. 5.2.

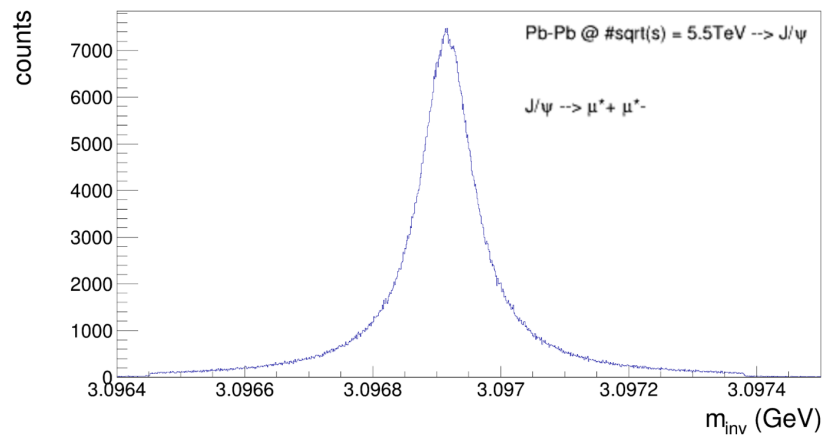| $l^\pm$	p_T	using eq. 5.15	σ_{p_T}	σ_m
$\mu^\pm$	$(1.444 \pm 0.117)\text{GeV}$	$1.547 \pm 5.6 \cdot 10^{-5}$ GeV	<1	0
$e^\pm$	$(1.447 \pm 0.117)\text{GeV}$	$1.548 \pm 5.6 \cdot 10^{-5}$ GeV	<1	0

Table 5.2: Comparison of the simulated and calculated value of the momentum.
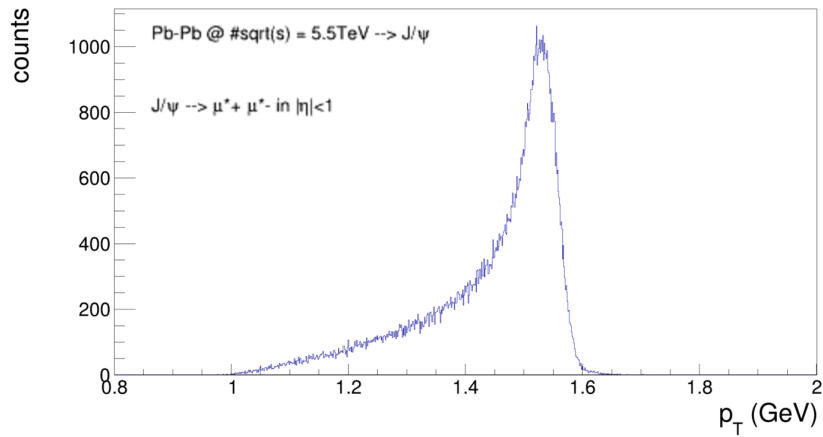
(a)

(b)

(c)

Figure 5.1: The figures are generated with the TLorentzVector class from root, regarding the $J/\psi \to \mu^+\mu^-$ decay channel
a) p_T spectrum of the muons transversing in $|\eta| < 1$ direction; b) the p_T spectrum of the J/ψ-meson; c) the mass of the J/ψ following a Breit-Wigner distribution.

The calculations were performed to cross-check the data sampling.

Figure 5.1 shows the mass and p_T distribution of the muons and their originating J/ψ's. The muon p_T spectrum peaks at half of the J/ψ's rest mass, the small deviations occur due to the small p_T-values of the mother particle as shown in figure 5.1 c). The p_T distribution of the J/ψ follows the same distribution analyzed in [3]. The peak is located at the typical energy scale $\sim 1/R_{AA}$, R_{AA} representing the size of the nucleus. In this case, this converts to about 30MeV for the lead nucleus. The small bump located above 100MeV originates from the scattering of one of the nucleons inside the nucleus used. This is called coherent and incoherent production, respectively. Compared to the luminosity of $L = 233\mu\mathrm{b}^{-1}$ in[3], the luminosity for Run 3 and 4 is higher by a factor 43, resulting in higher statistics than at the time [3] was published.

"STARlight" calculates the final cross-section for the J/ψ production integrated for all rapidity values. The previously described detector systems that are used in Run 3 (2022-2025) and Run 4 (2029-2032) work in a pseudorapidity range from $|\eta| < 1$. A corresponding cut has to be made for the lepton pairs, due to the possibility of leptons decaying outside of the rapidity cut, if only a cut for the J/ψ's is made.

All leptons which do not follow the condition are sorted out so that only the detectable pairs remain. Finally, a percentage of how many events follow this condition is obtained. To get the number of photons this has to be taken into account. Figure 5.2 shows the spectrum of the cut that was prepared for this purpose.

$l^\pm$	Pb-Pb $\sqrt{s_{NN}} = 5.5\mathrm{TeV}$	pp $\sqrt{s_{NN}} = 13.6\mathrm{TeV}$
σ	41.645mb	80.682nb
$\sigma \cdot BR(e^+e^-)$	2.487mb	4.818nb
$\sigma \cdot BR(\mu^+\mu^-)$	2.482mb	4.810nb
$\sigma_{e^\pm \mathrm{in} |\eta|<1}$	0.287mb	0.325nb
$\sigma_{\mu^\pm \mathrm{in} |\eta|<1}$	0.286mb	0.324nb

Table 5.3: The total cross-section calculated by "STARlight" with the number of lepton pairs decaying into mid-rapidity direction per leptonic J/ψ decay.

The total cross section was also multiplied by the branching ratio for the leptonic decay channels [24]. Table 5.3 presents the lepton decay channel percentages, where both leptons decay in mid-rapidity. Dividing the number of event entries in the cut by the total number of events, the percentages for the detectable lepton pairs are received. Table 5.3 shows the total cross-section computed for the J/ψ production over the whole rapidity range, without the leptonic branching ratio taken into account for a variety of nucleus-nucleus collisions.
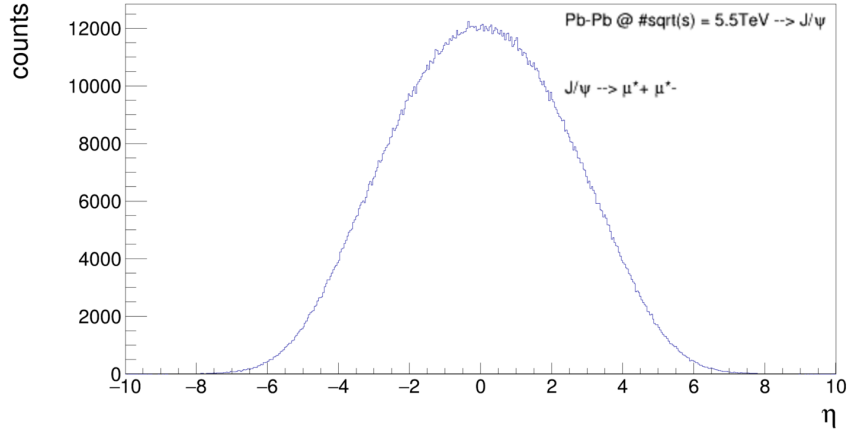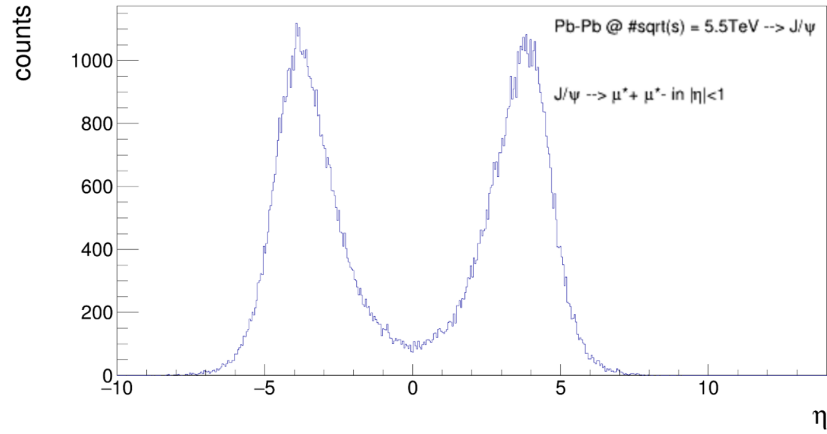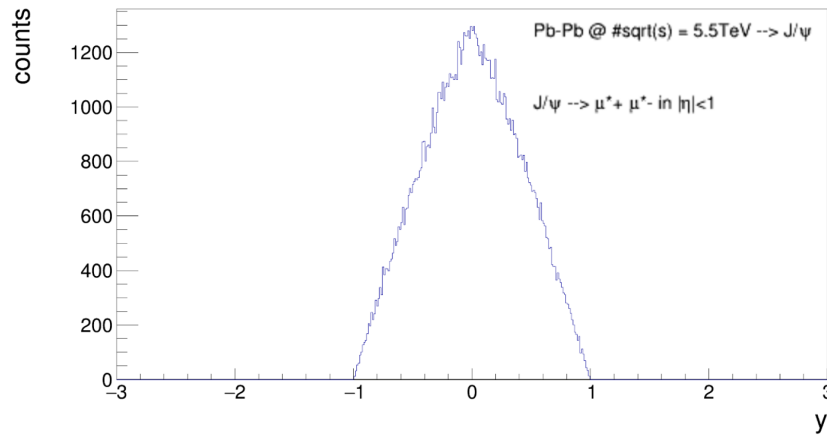
Figure 5.2: The Figure represents the whole pseudorapidity spectrum of the muon pairs in the decay process, following a Gaussian distribution.

(a)

(b)

Figure 5.3: a) represents the pseudorapidity range for the decaying meson for the case of the dimuon in the detectable eta region; b) shows the rapidity distribution of the J/ψ meson under the same condition.

Figure 5.2 presents the reason why a cut has to be made to get the right value for the percentage

of incident and detectable particles. "STARlight" generates the cross-section of the vector meson for the whole pseudorapidity range without taking the branching ratio into account. The energy of the J/ψ-meson is not much higher than the rest mass, being the reason for the dip in fig. 5.2 for the dimuon decaying in the desired η range. The stronger the peak in rapidity, the stronger the dip is in pseudorapidity range, for non-relativistic particles. This relation follows the approximation

$$y \approx \eta - \frac{tanh\eta}{s}\left(\frac{m}{p_T}\right)^2.$$

(5.18)

The lepton pairs fed through Low's formula are in the limit of $|\eta| < 1$.

5.2 Application of Low's Theorem

After "STARlight" generates the decaying dilepton information needed, it is stored in a TTree environment, where for every decaying J/ψ meson, the dilepton entries are kept the same.

A grid is filled using eq. 2.7 in order to get a representation of Low's formula. The following variables η and ϕ represent the pseudo-rapidity and azimuth angle in detector coordinates. The momentum of the photons is calculated by values inserted from the grid, with the formula looping over all possible entries between 0 and π for θ and 0 and 2π for ϕ totaling to one thousand bins, respectively. Corresponding in a total of one million possibilities for every dilepton. Since the interest lies in a figure that shows the dependence of the pseudorapidity η, the program is looping over all η−entries, which convert to values of θ. The resulting data for the photons is then stored with their associated lepton pair to distinguish them later on.

Depending on θ and ϕ, the photon-momentum entries are calculated and then inserted into the grid. The photon energy has to be set to a specific value to obtain a coherent plot, which can be changed nonetheless. This means that one can create the following figures Fig.5.4 and Fig.5.5 for every possible photon energy and beyond.

The photon momentum is calculated as follows:

$$\theta = 2 \cdot atan\left(e^{-\eta}\right) \tag{5.19}$$

$$p_x = cos(\phi) \cdot sin(\theta) \cdot E_\gamma \tag{5.20}$$
$$p_y = sin(\phi) \cdot sin(\theta) \cdot E_\gamma \tag{5.21}$$
$$p_z = cos(\theta) \cdot E_\gamma \tag{5.22}$$

$$p_{total} = \sqrt{\left(p_x^2 + p_y^2 + p_z^2\right)} = E_\gamma \tag{5.23}$$

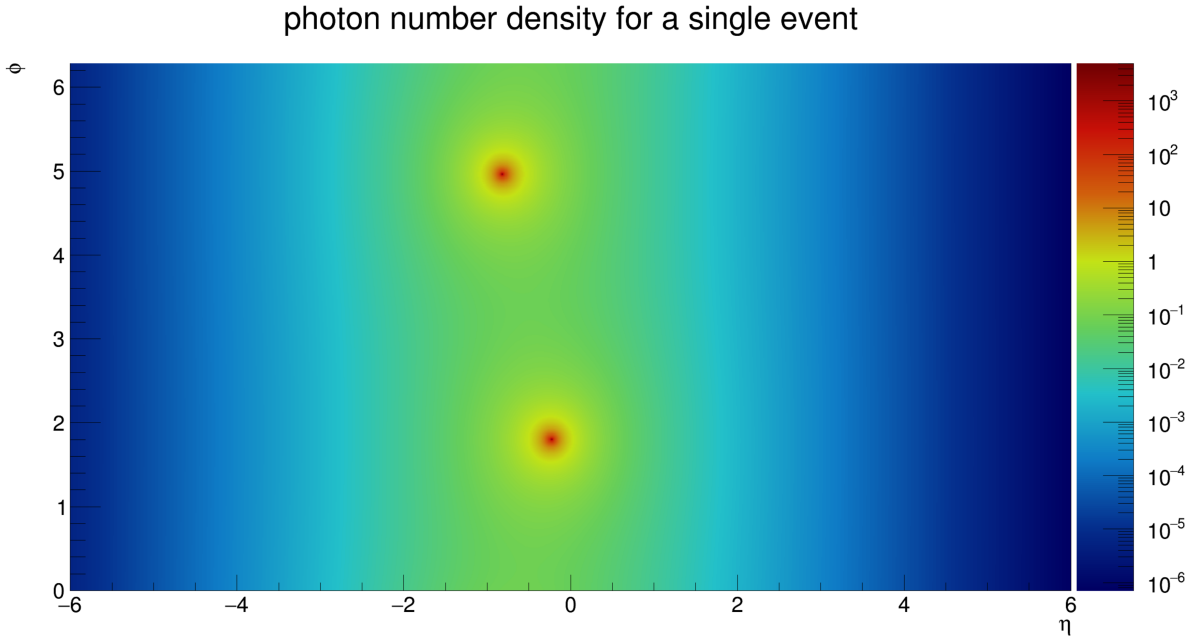For single events the grid looks as follows:

Figure 5.4: Photon density for one electron pair with $E_\gamma = 10\text{MeV}$ plotted as a heat map.
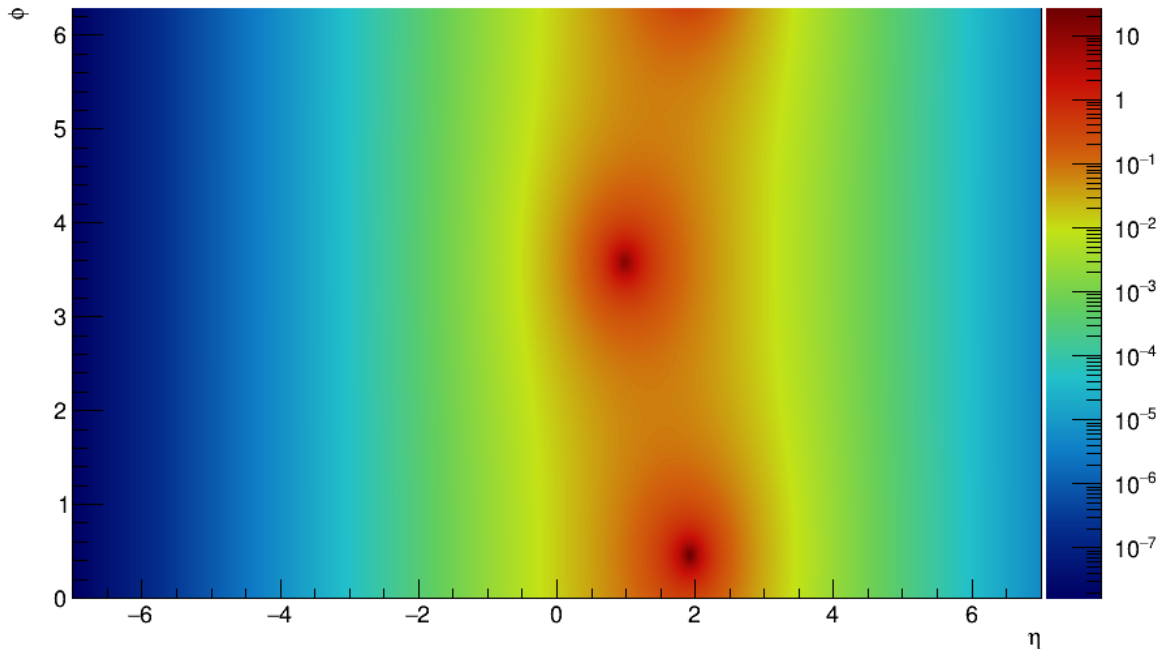
Figure 5.5: Photon density for one muon pair with $E_\gamma = 10\text{MeV}$ plotted as a heat map.

In figure 5.5 and 5.4, it is visible that the emitted bremsstrahlung photons are co-linear, the photons are traveling preferably in the same direction as the emitted charged particles. For the muon plot, a suppression near small angles can be observed, indicating the dead cone effect for the muon channel.

Analysis of Low's Theorem

The basic execution of the code is described in section 5.2. The figures in that section are not cut into the final frame, and the grating of the necessary grid for the division of the generated photon density is not fine enough.

The grating is set to a total of one million grid points reaching from zero to 2π on the y-axis and -1 to $+1$ on the x-axis ($\phi - \eta$ grid). For the following figures, the "STARlight" events are used to compile the figures. Per event, one million photon-density values are calculated, resulting in one billion total calculations for each plot. Thanks to the capability of "STARlight", cutting the dileptons into the desired pseudorapidity range, each considered muon is located in the region of $|\eta| < 1$. The run time for this execution is much longer than before, clocking in at over five hours for only one thousand $J/\psi \rightarrow l^+l^-$ events, with the dilepton decaying in the detectable limit. For the upcoming plot, ten thousand "STARlight" events were used for the computation.
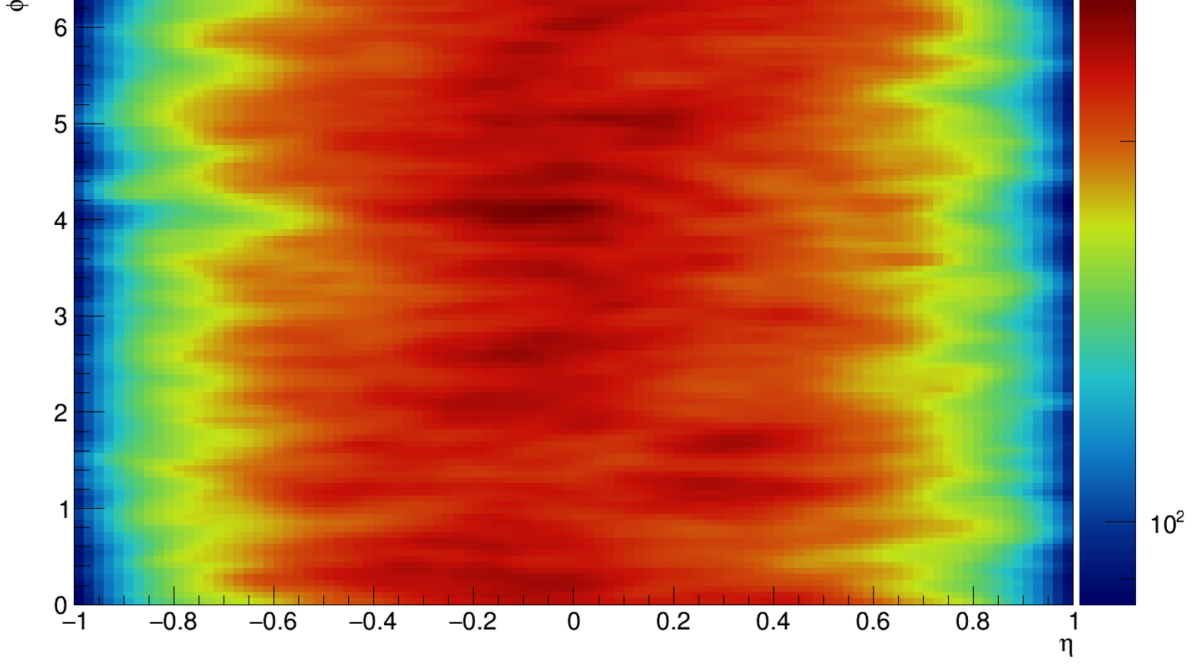
Figure 5.6: The photon density plotted for photons with the energy of $E_\gamma = 100\text{MeV}$ for the muon decay channel (the same figure can be made for the electrons).

The density of the photons for the electrons is higher compared to the muon density plot. The result is as expected from Low's theorem, which is also found in the generally higher radiation rate for the photons in the different decay channels.

The integral was calculated by counting all histogram entries with their width taken into account, using the TH2D integrate function in root. As mentioned previously, the photon number density by applying Low's formula only calculates it for one photon energy set. To get the total integrated number an integrating factor has to be multiplied. This factor reads

$$N = Integration(...) \cdot E_\gamma \cdot \ln\left(\frac{E_{max}}{E_{min}}\right). \tag{5.24}$$

The photon energy E_γ has to be multiplied to get a unitless expression since the total number of all energies is unitless. To compare the total number per event generated through root, the dN/dE_γ data is plotted in python. The final numbers of photons emitted in $|\eta| < 1$ direction with energies in the region of $E_\gamma \in [100\text{MeV}, 1.5\text{GeV}]$ are:

$$N_{J/\psi \to e^+e^-\gamma} \approx 0.1972 \text{ per } J/\psi \to e^+e^- \text{ decay}$$
$$N_{J/\psi \to \mu^+\mu^-\gamma} \approx 0.0652 \text{ per } J/\psi \to \mu^+\mu^- \text{ decay}.$$

One sees that the probability of an inner bremsstrahlung photon being emitted between muons and electrons is about 1/3, which is consistent with an analytical formula given below in eq. 5.2.
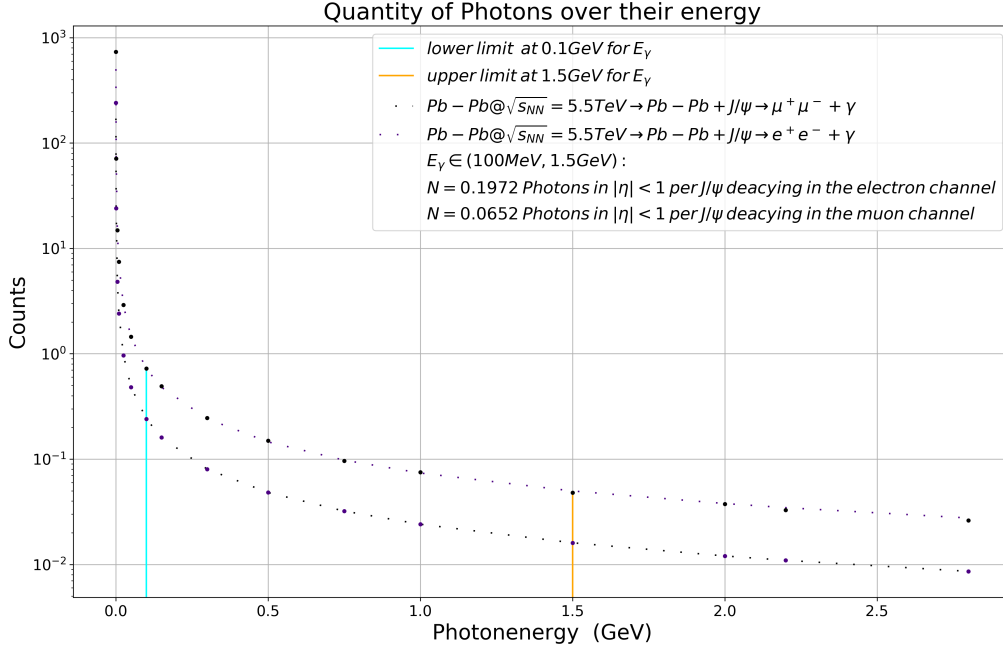
Figure 5.7: Spectrum of the integrated photon number density calculated with Low's theorem for e^+e^-- and $\mu^+\mu^-$- pairs.

The result from the Fermilab measurement [6], analyzing the $J/\psi \to e^+e^-$ reaction, states that the percentage of photons being emitted with an energy $E_\gamma > 100$MeV is 0.147 ± 0.022, which is nearly half of the value generated using Low's theorem. The cut made for the Fermilab observation was in θ_1 and $\theta_2 \in [15, 60]$ direction for the electrons and photons. The difference results from the different incisions made in this work at $\theta \in [40.4, 139.6]$, which correspond to the mid-rapidity range with $\eta = -ln\left[tan\left(\frac{\theta}{2}\right)\right]$.

The ratio between the inner bremsstrahlung radiation of the muon and electron decay channel can also be compared with some theoretically highlighted data from the paper [4]. The ratio for radiated photons with an energy $E_\gamma > 100$MeV between the inner bremsstrahlung from electrons compared to muons is ≈ 3. Even if it would be theoretically possible to measure photons down to the upper energy limit for pair conversion discussed in Sec. 4, the ratio would still be set at a value of approximately 3.

The fraction of photons emitted with the energy E_{min} was analytically calculated by [4].

$$C_{\text{hard}}\ (E_{\text{min}}) = \frac{\alpha}{2\pi}\left[4\ln\frac{M}{2E_{\text{min}}}\left(\ln\frac{M^2}{m_l^2} - 1\right) - 3\ln\frac{M^2}{m_l^2} - \frac{2}{3}\pi^2 + \frac{11}{2}\right]. \tag{5.25}$$

The ratio is stated to be of a factor 2.6 between the leptonic decay channels of the J/ψ meson. Since the paper states that for the leading order term, it is assumable that the photon energies considered are not yet low enough for the leading order of the process 2.1 to dominate the interaction.

The integrated ratio for different minimal photon energies E_γ is plotted with the formula for the inner bremsstrahlung percentage eq. 5.2 in fig. 5.8. The final number of photons emitted per event in the $J/\psi \to l^+l^-$ decay channel are as well summed up in eq. 5.24.

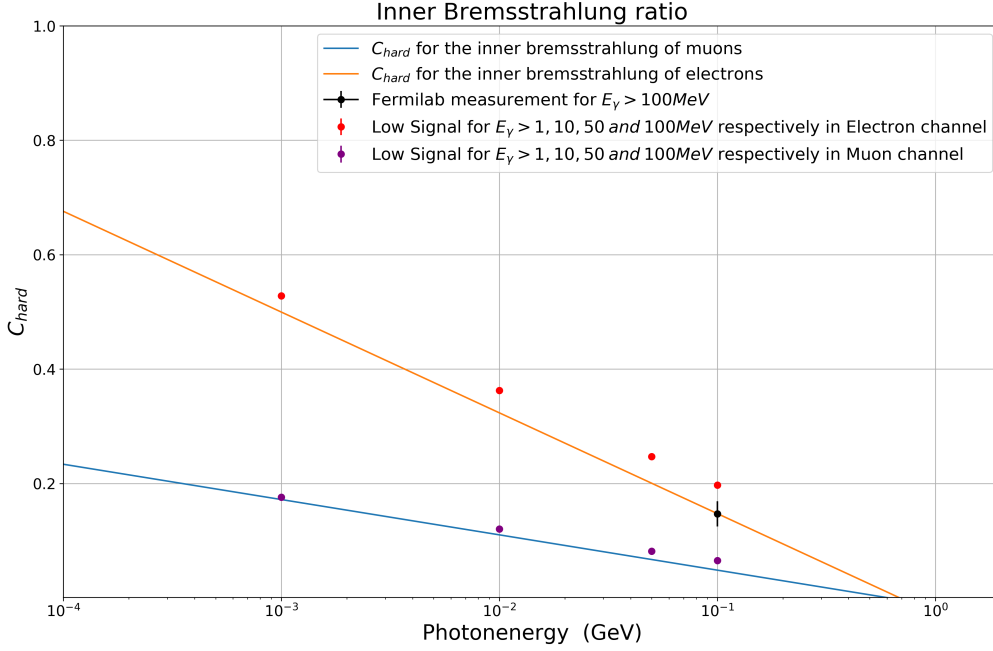Figure 5.8: The theoretical inner bremsstrahlung C_{hard} [4] plotted with the bremsstrahlung ratio for different lower limits for E_γ using Low's Formula.

Low Signal

The radiation of massless gauge bosons by a spin $1/2$ fermion is suppressed in an angular region in the direction of the emitting charged fermion in a region $\theta \sim m/E$ for QED and QCD. This region is commonly denoted as the dead cone [42]. The dead cone effect is investigated by plotting the angular distribution of emitted photons against the photon density number accessible by the information gathered by STARlight and Low's Formula eq. 2.7. The angle is calculated with three-vector momenta of the lepton and the photon:

$$\vec{p_l} \cdot \vec{p_\gamma} = |\vec{p_l}| \cdot |\vec{p_\gamma}| \cos \Theta_{l-\gamma} \tag{5.26}$$

$$\cos \Theta_{l-\gamma} = \frac{\vec{p_l} \cdot \vec{p_\gamma}}{|\vec{p_l}| \cdot |\vec{p_\gamma}|} \tag{5.27}$$

Inserting the energy-momentum relation $E^2 = p^2 c^2 + (mc^2)^2$ and setting the light-speed $c = 1$, the energy and mass dependence is observable

$$\cos \Theta_{l-\gamma} = \frac{\vec{p_l} \cdot \vec{p_\gamma}}{E_\gamma \cdot \sqrt{E_\mu^2 - m_\mu^2}} \tag{5.28}$$

$$\approx \frac{1}{E_\gamma E_\mu} \cdot \vec{p_l} \cdot \vec{p_\gamma} \tag{5.29}$$

The angle is plotted against the photon number density calculated for the respective photon and lepton pair using Low's theorem in fig. 5.6.
The same can be done for the electrons. Since the mass of the electron is smaller by a factor of about two hundred, the dead cone effect is much more difficult to observe. This is observable in fig. 5.9, where both the zoomed-in electron and muon distribution are plotted. The muon

distribution follows a suppression for small angles while the electron dead cone effect is not visible due to the rapid decline. The angle $\theta \sim m/E$ of the muon dead cone effect at around ~ 0.07 is observable in 5.9.
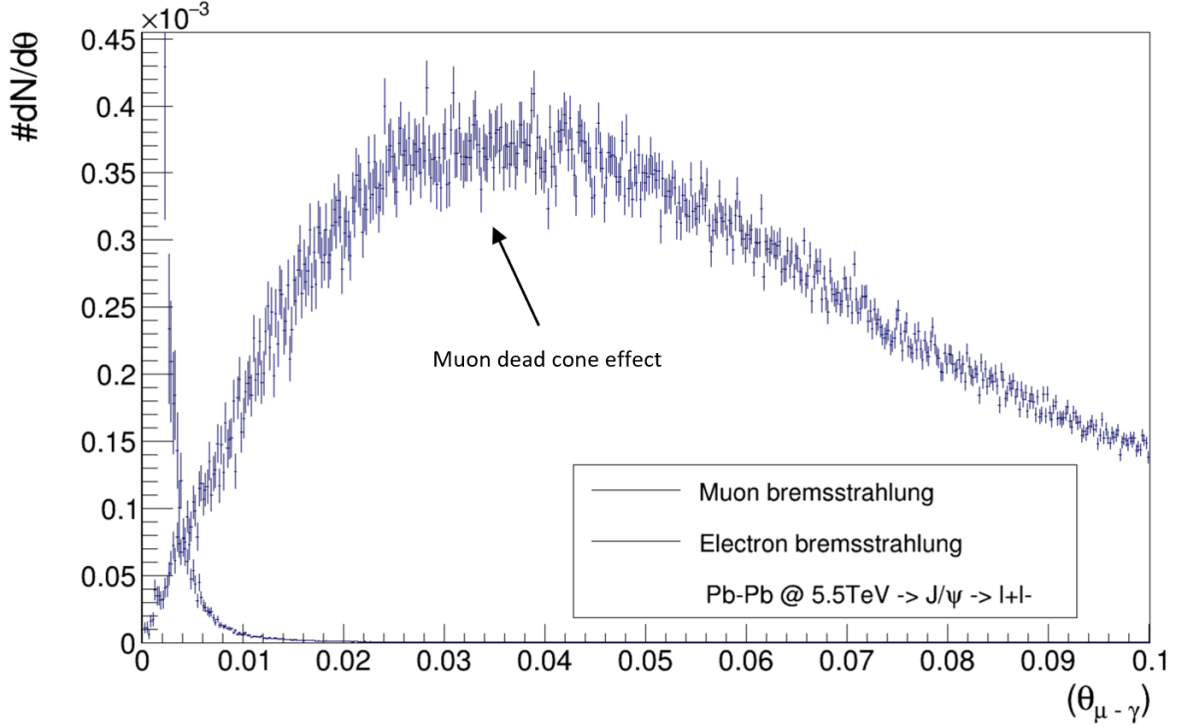

Figure 5.9: Combined zoomed-in dead cone effect of muons and electrons.

Taking everything so far into account, the final result of how many detectable photons are in the mid-rapidity region ($|\eta| < 1$) is summed up in the following tables 5.4 and 5.5. The total photon number N_γ is calculated by multiplying the visible cross-section $\sigma_{l\pm \text{in } |\eta|<1}$ with the branching ratio [24], the number of photons per event n_γ at 5.24, the detector efficiency $\xi \sim 0.15$ of the e^+e^- pair from the photon interaction discussed in Sec. 4 [44], the tracking efficiency of 0.9 per track of the decay lepton from the J/ψ [43] and the percentage of the lepton pairs in the detectable region ϵ from tab. 5.3. For the integrated luminosity for the Pb-Pb collision, a value of $L_{int} = 10\text{nb}^{-1}$ is used [5]. For the pp collision $L_{int} = 200\text{pb}^{-1}$ [5]. In the end, the photon conversion rate is multiplied by the probability of the emitted photon being converted in an electron-positron pair in the TPC $P_{TPC} \sim 4.6\%$ [43]:

$$N_{J/\psi \to l^+l^-} = \sigma_{l\pm in|\eta|<1} \cdot L_{int} \tag{5.30}$$

$$N_\gamma = N_{J/\psi \to l^+l^-} \cdot Eff_{Tracking}^2 \cdot n_\gamma \tag{5.31}$$

$$N_{\gamma\,final} = N_\gamma \cdot P_{TPC} \cdot \xi. \tag{5.32}$$

The outcomes regarding ALICE Run 3 and 4 statistics are summed up for lead-lead collisions in the following table taking the result from tab. 5.3 into account. The square root of $N_{\gamma\,final}$ is used as the statistical deviation for it.

Pb-Pb$\rightarrow J/\psi$	$J/\psi \rightarrow e^+e^-$	$J/\psi \rightarrow \mu^+\mu^-$
L_{int}	10nb^{-1}	10nb^{-1}
$\sigma_{l\pm in|\eta|<1}$	0.287mb	0.286mb
$N_{l\pm\ |\eta|<1}$	$2.87 \cdot 10^6$	$2.85 \cdot 10^6$
$N_{l\pm\ |\eta|<1} \cdot Eff^2_{Tracking}$	$2.32 \cdot 10^6$	$2.31 \cdot 10^6$
N_γ	457504	150612
$N_\gamma \cdot$ TPC	21045	6928
$N_{\gamma\ final}$	3156 $\pm$56	1039 $\pm$31

Table 5.4: The material budget of the beampipe and ITS2 of 6% leads to a TPC conversion probability of 4.6%; The final number of detectable Photons in an energy region from 100MeV to 1.5GeV in Pb-Pb collisions with Run 3 + 4 statistics applied.

$pp \rightarrow J/\psi$	$J/\psi \rightarrow e^+e^-$	$J/\psi \rightarrow \mu^+\mu^-$
L_{int}	200pb^{-1}	200pb^{-1}
$\sigma_{l\pm in|\eta|<1}$	0.325nb	0.324nb
$N_{l\pm\ |\eta|<1}$	65000	64800
$N_{l\pm\ |\eta|<1} \cdot Eff^2_{Tracking}$	52650	52488
N_γ	10382	3422
$N_\gamma \cdot$ TPC	477	157
$N_{\gamma\ final}$	71$\pm$8	23$\pm$4

Table 5.5: The material budget of the beampipe and ITS2 of 6% leads to a TPC conversion probability of 4.6%; the final number of detectable Photons in an energy region from 100MeV to 1.5GeV in pp collisions with Run 3 + 4 statistics applied.

5.3 Experimental Background

To make a final statement if the measurement is feasible with the complete Run 3 and Run 4 data set, the signal from fig. 5.7 can be compared to the external bremsstrahlung radiation in the detector geometry. The external bremsstrahlung is emitted by the lepton pairs from the J/ψ decay while propagating through the detector material.
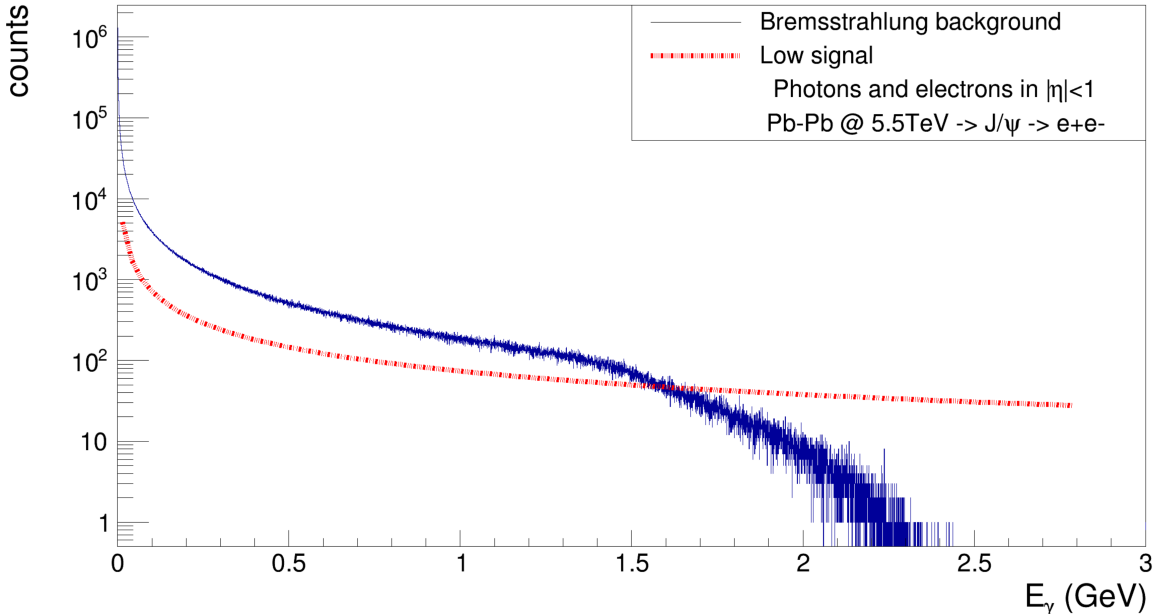

Figure 5.10: Emitted background photons in GeV for e^+e^- pairs with logarithmic y-scale plotted against the spectrum obtained by Low's Formula.
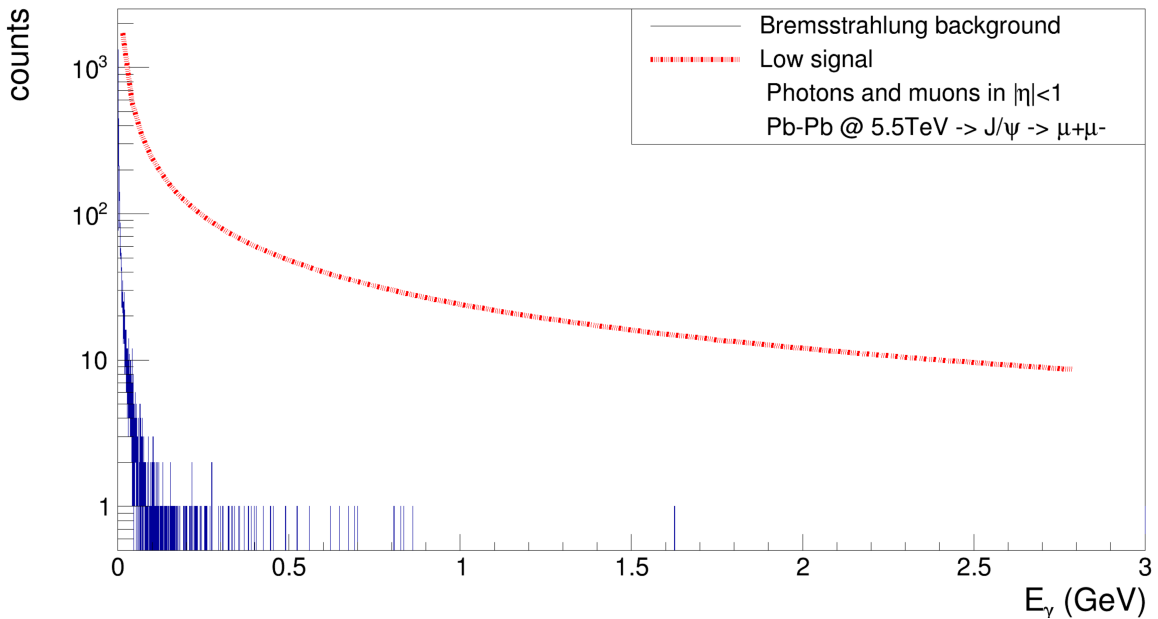

Figure 5.11: Emitted background photons in GeV for $\mu^+\mu^-$ pairs with logarithmic y-scale plotted against the spectrum obtained by Low's Formula.

The external bremsstrahlung of charged particles is suppressed by $1/m^4$. Inner bremsstrahlung

does not show this suppression and is instead only dependant on the relativistic velocity β seen in eq. 2.7. The equation also shows that no maximum value for the photon energy is given. The cut, or rather the upper limit for this observation is arbitrarily set at 1.5GeV, where the kinematic limit leads to a severe deviation from this functional form. The kinematic limit of the electron decay channel is higher because of the lower mass of the electron. For comparison, the upper limit is set at the same value.

The counts of the electron background radiation is comparatively higher than the spectrum obtained by the integrated Low formula, making it challenging to distinguish the signals from the detector background and Low to analyze the soft photons radiated in the J/ψ decay. On the other hand, the muon background radiation is nearly negligible, compared to the simulated counts. The background radiation was computed with 1 million lepton pairs, each taken into account. To successfully measure soft photons, the muon decay channel is strongly suggested.

The background signal occurring during the interaction, where the J/ψ is being produced, was not taken into account. The dominant contribution is the direct dimuon production of UPC, discussed in further detail in [15] [3] in general and in respect to the production of the J/ψ-vector meson, shown in fig. 5.12. This continuum of non-resonant dimuon production has an even larger cross-section than the J/ψ to dimuon production cross-section and might serve as a complementary measurement for inner bremsstrahlung.

The background resulting from this is shown in fig. 5.12 taken from the coherent J/ψ production in UPC in [3].
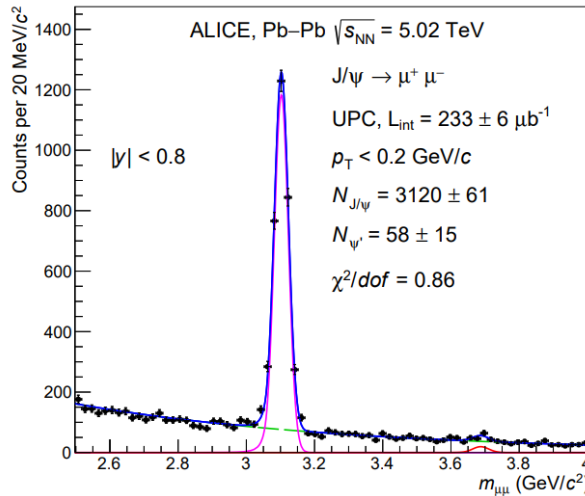

Figure 5.12: Invariant mass distribution of $\mu^+\mu^-$ pairs. The dashed green line corresponds to the non-resonant $\mu^+\mu^-$ pair production background. The solid blue line corresponds to the sum of background and signal functions [3].

ALICE 3 statistics

In order to get a glimpse of the possibilities of the future ALICE 3 experiment, the calculations for the Run 3 and Run 4 set-up can be made for the 2032 detector system, which will cover a pseudorapidity range of $|\eta| < 4$. The values for the energies and the luminosities are taken from [2].

$l^{\pm}$	Pb-Pb $\sqrt{s_{NN}} = 5.52\text{TeV}$	pp $\sqrt{s_{NN}} = 14\text{TeV}$	Kr-Kr $\sqrt{s_{NN}} = 6.46\text{TeV}$	O-O $\sqrt{s_{NN}} = 7\text{TeV}$
σ	41.761mb	82.293nb	2.974mb	27.49μb
$\sigma \cdot BR(e^+e^-)$	2.494mb	4.914nb	0.1776mb	1.641μb
$\sigma \cdot BR(\mu^+\mu^-)$	2.489mb	4.905nb	0.1773mb	1.639μb
L_{month} (nb^{-1})	5.6	$5.1\cdot10^5$	$8.4\cdot10^1$	$1.6\cdot10^3$
$\sigma_{e^{\pm} in |\eta|<4}$	2.049mb	2.843nb	0.143mb	1.262μb
$N_{e^{\pm} \, |\eta|<1}$	$11.5 \cdot 10^6$	$1.45 \cdot 10^6$	$12.0 \cdot 10^6$	$2.02 \cdot 10^6$
$\sigma_{\mu^{\pm} in |\eta|<4}$	2.044mb	2.836nb	0.142mb	1.260μb
$N_{\mu^{\pm} \, |\eta|<1}$	$11.5 \cdot 10^6$	$1.45 \cdot 10^6$	$11.9 \cdot 10^6$	$2.02 \cdot 10^6$

Table 5.6: The total cross-section calculated by "STARlight", the number of lepton pairs decaying into $|\eta| < 4$ direction per leptonic J/ψ decay with the Luminosities taken from ALICE 3 configurations.

The total number of photons generated per leptonic J/ψ decay in an energy range of $E_\gamma \in (100\text{MeV}, 1.5\text{GeV})$ is respectively:

$$N_{J/\psi \to e^+e^-\gamma} \approx 0.2284 \text{ per } J/\psi \to e^+e^- \text{ decay}$$
$$N_{J/\psi \to \mu^+\mu^-\gamma} \approx 0.0861 \text{ per } J/\psi \to \mu^+\mu^- \text{ decay.}$$

For the ALICE 3 computation the photons are also radiated in $|\eta| < 4$ direction. The ratio for the larger rapidity range is calculated as ≈ 2.65, meaning that it got closer to the theoretical value of 2.6 [4]. The number of inner bremsstrahlung photons is not estimated, since the computations for the ALICE 3 detector efficiencies are not fully completed yet.

Section 6

Conclusion and Outlook

The aim of this work was to estimate the number of reconstructed inner bremsstrahlung photons from J/ψ decays in the leptonic channels for the ALICE experiment. The leptonic decay channel of the J/ψ's produced in ultra-peripheral collisions was considered. In the course of the analysis, the range of the simulated particles was adjusted to the detector limits, which corresponds to the mid-rapidity region of $|\eta| < 1$. The clean separation between the electrons and muons has already been achieved with the TPC in ultra-peripheral collisions, which supports the analysis of the inner bremsstrahlung photons. The decaying lepton particles from the J/ψ were generated with the event generator "STARlight". The information obtained was used in combination with Low's formula to estimate the photon yield in the mid-rapidity region. It shows that the photon yield is by a factor of three smaller than for electrons. This results from the velocity β having a different weight in the Low theorem for electrons and muons. The photon spectra, as calculated with Low's theorem, are in fair agreement with the analytical calculations. However, small deviations may point to the fact that the chosen minimum photon energy of 100MeV is still not sufficiently small enough for the Low theorem to hold true.

The experimental background for the transversing electrons emerging from external bremsstrahlung in the detector material is about ten times larger than the signal induced from the $J/\psi \rightarrow e^+e^-$ decay, likely prohibiting such a measurement. Compared to the electron signal, the external background radiated by the muons is negligible in contrast to the inner bremsstrahlung spectrum. This is a consequence of the larger mass of the muon. This makes the muon channel approximately background free and qualifies for a golden channel to be looked at with the complete Run 3 and 4 data set. The estimated number of about 1000 detected inner bremsstrahlung photons might be reduced by a factor of up to two in case of strong shadowing effects in the gluon distribution of the lead nuclei, which was not considered in this thesis.

Estimates for the cross-sections and the number of photons emitted per leptonic decay in $|\eta| < 4$ direction are also given for the ALICE 3 detector that is presently planned to be installed in 2033. While the acceptance of J/ψ detection in the leptonic decay channels is increased by a factor of 7, the detected number of inner bremsstrahlung photons is still to be worked out, since the computations for the photon detection are not fully completed yet.

Bibliography

[1] F.E. Low, Bremsstrahlung of Very Low-Energy Quanta in Elementary Particle Collisions, et al. Physics Review 110:974 (1958).

[2] Alice Collaboration, Letter of intent for ALICE 3: A next-generation heavy-ion experiment at the LHC, doi.org/10.48550/arXiv.2211.02491 (2022).

[3] ALICE Collaboration, Coherent J/ψ and ψ' photoproduction at midrapidity in ultra-peripheral Pb-Pb collision at $\sqrt{s_{NN}} = 5.02$TeV, arXiv:2101.04577v2 [nucl-ex] 9 Dec 2021.

[4] Alexander Spiridonov, Bremsstrahlung in Leptonic Onia Decays: Effects on Mass Spectra, arXiv:hep-ex/0510076 (2005).

[5] Johannes Stiller, Full kinematic reconstruction of charged B mesons with the upgraded Inner Tracking System of the Alice Experiment, PhD Thesis (2016).

[6] FERMILAB Collaboration, Observation of the radiative decay $J/\psi \rightarrow e^+ e^- \gamma$, Phys. Rev. D Vol. 54 Nr. 11, p. 7067-7070 (1996).

[7] ALICE Collaboration, ALI-PUBALI-48827.

[8] C.Y. Wong, An Overview of the Anomalous Soft Photons in Hadron Production, arXiv:1404.0040v1 (2014).

[9] J. Abdallah et al., (DELPHI Collaboration), Eur. Phys. J. C67, 343 (2010).

[10] J. Abdallah et al. (DELPHI Collaboration), Eur. Phys. J. C47, 273 (2006).

[11] L. Van Hove, Ann. Phys. (N.Y.) 192, 66 (1989); P. Lichard and L. Van Hove, Phys. Lett. B245, 605 (1990); P. Lichard, Phys. Rev. D50, 6824 (1994).

[12] W. Czyz and W. Florkowski, Z. Phys. C61, 171 (1994).

[13] Fermi E Z. Physik 29:315 (1924).

[14] Weizsäcker CF Z. Physik 88:612 (1934); Williams EJ Phys. Rev. 45:729 (1934).

[15] C.A. Bertulani, S.R. Klein and J. Nystrand, Physics of Ultra-Peripheral Nuclear Collisions, Ann.Rev.Nucl.Part.Sci.55:271-310doi.org/10.1146/annurev.nucl.55.090704.151526 (2005).

[16] Frankfurt L, Strikman M and Zhalov M, Phys. Lett. B 540:220 (2002).

[17] Klein SR, Nystrand J Phys. Rev. Lett. 84:2330 (2000); Phys. Lett. A 308:323 (2003).

[18] J. E. August, Discovery of a Narrow Ressonance in $e^+ e^-$ Annihilation, Phys. Rev. Lett. 33, pp. 1406–1408. doi: 10.1103/PhysRevLett.33.1406 (1974).

[19] J. J. Aubert et al. "Experimental Observation of a Heavy Particle J". In: Phys. Rev. Lett. 33, pp. 1404–1406; doi.org/10.1103/PhysRevLett.33.1404 (1974).

[20] The Royal Swedish Academy of Sciences. https://www.nobelprize.org/prizes/physics/1976/press-release/ (1976).

[21] V.V. Anashin, and others, Measurement of $\Gamma_{ee}(J/\psi)$ with KEDR detector, JHEP 05, arXiv:1801.01958v1 (2018).

[22] J. Z. Bai and others, A Measurement of J / psi decay widths, Phys. Lett.B 255 373-380, doi.org/10.1016/0370-2693(95)00712-T, 10.1016/0370-2693(95)01220-2 (1995).

[23] A. Boyarski and others, The Quantum Numbers and Decay Widths of the psi (3095), Phys.Rev.Lett 34, 10.1103/PhysRevLett.34.1357 (1975).

[24] Particle Data Group. cc Mesons. https://pdg.lbl.gov/2017/tables/rpp2017- tabmesons-c-cbar.pdf (2017).

[25] The CERN accelerator complex, http://cds.cern.ch/record/1260465?ln=en (2015).

[26] Alice Collaboration, Technical Design Report for the Upgrade of the ALICE Inner Tracking System, J. Phys. G 41 (2014) 087002 (2014).

[27] H. Bethe und J. Ashkin in "Experimental Nuclear Physics, ed. E. Segré, J. Wiley, New York, p. 253 (1953).

[28] M. Tanabashi et al. (Particle Data Group), Phys. Rev. D 98, 030001, Fig. 34.15 (2018).

[29] Alice collaboration, Performance of the ALICE Time-Of-Flight detector at the LHC, arXiv:1806.03825v1 (2018).

[30] Pietro Cortese and for the ALICE Collaboration, J. Phys.: Conf. Ser. 1162 012006 (2019).

[31] Wolfgang Demtröder. Experimentalphysik 4. Kern-, Teilchen- und Astrophysik. Springer-Verlag GmbH Berlin Heidelberg. isbn: 978- 3-662-52883-9 (2017).

[32] D.E. Groom and S.R. Klein, Passage of Particles Through Matter, https://pdg.lbl.gov/2022/reviews/contents_sports.html [last accessed 13-November-2022].

[33] J. H: Hubbel, Review of photon interaction cross section data in the medical and biological context, Phys. Med. Biol 44 R1-R22.

[34] S. R. Klein, STARlight: A Monte Carlo simulation program for ultra-peripheral collisions of relativistic ions, arXiv:1607.03838v2 [hep-ph] (2016).

[35] C. A. Bertulani, S. R. Klein and J. Nystrand, Ann. Rev. Nucl. Part. Sci. 55, 271 (2005); G. Baur et al., Phys. Rept. 364, 359 (2002); F. Krauss, M. Greiner and G. Soff, Prog. Part. Nucl. Phys. 39, 503 (1997); A. J. Baltz et al., Phys. Rept. 458, 1 (2008).

[36] C. W. deJager, H. deVries and C. deVries, At. Data Nucl. Data Tables 14, 495 (1974).

[37] J. Nystrand and S. Klein, preprint arXiv:9811007 (1998).

[38] K. A. Olive et al. [Particle Data Group], Chin. Phys. C38, 090001 (2014).

[39] J. A. Crittenden, Exclusive Production of Neutral Vector Mesons at the Electron-Proton Collider HERA, Springer-Verlag, Berlin (1997).

[40] TLorentzVector class in root [last checked 8.12.2022].

[41] R.L. Workmanet al.(Particle Data Group), Prog.Theor.Exp.Phys.2022, 083C01 (2022).

[42] DELPHI collaboration, Observation of the muon inner bremsstrahlung at LEP1, Eur. Phys. J. C 57: 499–514 (2008).

[43] F. Reidt on behalf of the ALICE collaboration, Upgrade of the ALICE ITS detector, arXiv:2111.08301v3 [physics.ins-det] (2022).

[44] ALICE Collaboration, Performance of the ALICE Experiment at the CERN LHC, arXiv:1402.4476 (2015).
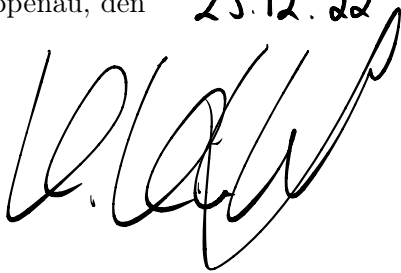
Acknowledgements

Declaration

I declare that I have written this thesis by myself and used no other sources or aids than those indicated.

Oppenau, den 23.12.22